People`s Democratic Republic of Algeria
Ministry of Higher Education and Scientific Research
University of Echahid Hamma Lakhdar - El Oued
Faculty of Technology
Department of Process Engineering & Petrochemistry

Dissertation

ACADEMIC MASTER

Domain: Science and Technology

Division: Process Engineering

Specialty: Chemical Engineering

Presented by:

1. Ferhat Abderraouf
2. Abbassi Kodes
3. Abadi Raouia

Entitled:

Theoretical Study of Graphene and its Thermal Properties

Dissertation Submitted in Partial Fulfillment of the Requirements for the Master

Publicly defended in: 27/05/2025

Board of Examiners:

Dr. Segueni Leila	**Chairman**
Dr. Sek Lakhdar	**Supervisor**
Dr. Benmya Omar	**Examiner**

Academic Year: 2025/2024

Abstract

In this work, we explore the quantum and thermodynamic behavior of graphene placed in a uniform magnetic field while embedded within a curved Anti-de Sitter (AdS) spacetime. Treating the low-energy excitations as massless Dirac fermions, we apply the Nikiforov–Uvarov method to solve the resulting Dirac equation, yielding exact analytical solutions for both the energy levels and wavefunctions. These solutions clearly reflect how curvature and interaction strengths affect the system, leading to noticeable shifts and splitting in the Landau levels as a consequence of the AdS background. With the energy spectrum in hand, we proceed to formulate the system's partition function and derive thermodynamic quantities such as free energy, internal energy, entropy, and heat capacity. The results illustrate how curvature, combined with interaction effects, plays a decisive role in shaping the thermal properties—highlighting phenomena like divergences and signs of thermal instability. Overall, the study deepens our understanding of how graphene-like Dirac systems behave under curved spacetime conditions and sheds light on broader aspects of quantum field theories in deformed geometric settings.

الملخص

في هذا العمل، نستكشف السلوك الكمومي والديناميكي الحراري للجرافين الموضوع في مجال مغناطيسي منتظم أثناء وجوده داخل زمكان منحني من نوع(Anti-de Sitter (AdS . من خلال اعتبار الاستثارات منخفضة الطاقة كفرميونات ديراك عديمة الكتلة، نطبّق طريقة نيكيفوروف–أوفاروف لحل معادلة ديراك الناتجة، مما يؤدي إلى حلول تحليلية دقيقة لكل من مستويات الطاقة ودوال الموجة. تعكس هذه الحلول بوضوح كيف تؤثر الانحناءات وقوة التفاعلات على النظام، مما يؤدي إلى انزياحات وانقسامات ملحوظة في مستويات لانداو نتيجة خلفية .AdS بعد الحصول على طيف الطاقة، نتابع بصياغة دالة التقسيم للنظام واستنتاج الكميات الديناميكية الحرارية مثل الطاقة الحرة، والطاقة الداخلية، والإنتروبيا، والسعة الحرارية. توضح النتائج كيف أن الانحناء، بالتزامن مع تأثيرات التفاعل، يلعب دورًا حاسمًا في تشكيل الخصائص الحرارية—مبرزًا ظواهر مثل التشعبات وعلامات عدم الاستقرار الحراري. بشكل عام، يُعمّق هذا البحث فهمنا لكيفية تصرف أنظمة ديراك الشبيهة بالجرافين في ظروف الزمكان المنحني، ويسلط الضوء على جوانب أوسع في نظريات الحقل الكمومي في الأوساط الهندسية المشوهة.

DEDICATION

Praise be to Allah, whose blessings lead to the completion of good deeds. To Him belongs all favor, first and last, in successfully completing this thesis. Praise be to Him as is befitting His majesty and great sovereignty.

I dedicate this graduation to those whose prayers illuminated my path like lamps in the darkness of my journey... to my first supporter, my dear father. May Allah grant your health, wellness, and long life.

To the one who instilled values in me, whose constant prayers and helping hand never cease to extend good—my beloved mother. May Allah reward you with goodness and satisfaction.

To everyone who sincerely and faithfully taught me throughout my academic journey, nurturing in me a love of knowledge and striving to enlighten my mind—to my esteemed teachers. May Allah reward you with abundant goodness.

To those who surrounded me with genuine support and shared all my moments with love and care—my dear sisters.

To the one who shared work moments with me, who was my partner in achieving this accomplishment—my dear companion, Kodus.

To my supervisor, Dr. Sek Lakhdar, my sincere gratitude and appreciation for your efforts, generous guidance, and mentorship. I pray Allah grants you the best reward and blesses your knowledge and work.

Rawia Abadi

In the name of Allah, the Most Gracious, the Most Merciful. Praise be to Allah, the Lord of the worlds, who granted us strength and helped us complete this research in its

current excellent form. Just yesterday, we began our educational journey looking at graduation day as if it were a distant dream. We saw chemical engineering as a noble goal, a great adventure, and an aspiration worth enduring hardship and perseverance to achieve.

This research, which I present to you, carries within its pages valuable information that required tremendous effort to study and compile, ultimately resulting in its current form.

Believing in the principle that one does not thank Allah properly unless he thanks people, I would like to express my sincere gratitude to my supervising professor, Dr. Sek Lakhdar, for the valuable guidance and insightful information he provided, significantly enriching our study in various aspects.

Thanks, and Appreciation

To Allah, before all else...

All praise be to You, Allah, as befits the majesty of Your face and your great authority...

Praise be to Allah for the joy of achievement; praise be to Allah at the start and at the end.

With all my love, I dedicate the fruit of my success and graduation:

To my resilient self, who endured every stumble and continued despite difficulties. The journey wasn't short, nor should it have been. The dream wasn't close, nor was the path easy, but I did it and achieved it. Here I am today, standing at the threshold of my graduation, reaping the fruits of my efforts and proudly raising my cap. Praise be to Allah until You are pleased, praise be to You when You are pleased, and praise be to You after Your pleasure.

To my primary supporter, my backbone and strength after Allah, my pride and honor, my father who illuminated my paths and was my role model in every step I took. My father, my best support in fatigue and sadness, the shoulder on which I place my burdens. To my dear beloved, whom I love as much as this entire world—my heaven on earth.

To my pure angel and my strength after Allah, the one whose heart embraced me before her hands and who eased my hardships with her prayers. To the compassionate heart and the candle that lit my dark nights—my dear mother.

To my second mother, my husband's kind and caring mother, who supported me throughout my thesis journey. May Allah protect and care for her.

To those who supported me lovingly in my moments of weakness, removed obstacles from my path, paved the way, and instilled confidence and determination within me. To

my brothers, whom Allah strengthened my bond with—I pray Allah protects them: Omran, Ali, Othman, Abu Bakr Al-Siddiq.

To that man, my pillar, my soulmate who encouraged me to reach my ambitions, my support and life partner—my husband, Abdul Raouf.

To Zamzam, my beloved heart, my dear friend, my little and big sister.

To our little angel, my nephew—Taim.

To my companion on this journey of struggle, with whom honesty, effort, and determination made it possible to reach our goal. Half of this success truly belongs to you, Rawia, as does half of the gratitude.

Finally, I want to specially thank my supervisor and mentor, Dr. Sek Lakhdar, who deserves the most heartfelt thanks. You have been my first supporter and greatest motivator. Thank you for the patience you have shown us, the valuable knowledge, and the immense efforts you have contributed. May Allah bless you with health and wellness.

Abbasi Kodus

ACKNOWLEDGEMENTS

I dedicate my graduation, the fruit of my efforts, and the joy I have waited for my whole life to:

To my father, the love of my heart, may God have mercy on him.
To the one whom God graced with dignity and reverence.
To the one whose name I carry with pride.
To the one whose name is inseparable from mine.
To the source of support, giving, strength, and refuge after God.
To the one whose forehead bore the sweat of hard work,
who taught me that success comes only through patience and determination.
To the light that illuminated my path and the lamp whose glow will never fade in my heart.
To the one who gave everything, and from whom I drew my strength and self-worth…
My dear father.

To the unseen hand that removed the thorns from my path,
to the one who endured every moment of pain I went through and stood by me in times of weakness and hardship,
to the fountain of affection and compassion,
to the most wonderful woman in the world,
may God keep you with me for a lifetime…
My dear mother.

To those whom God blessed me with—the solid bond in my life,
my siblings.

To my life partner, who gave me strength and supported me at all times so I could become who I am today.

To my project supervisor, who never hesitated to extend a helping hand,

Dr. Sek Lakhdar.

Farhat Abdelraouf

TABLE OF CONTENTS

Table of Materials

LIST OF FIGURES

General Introduction

Graphene, a monolayer of carbon atoms arranged in a two-dimensional honeycomb lattice, is celebrated for its remarkable mechanical, electrical, and thermal properties. Since its isolation in 2004, graphene has stimulated intense interdisciplinary research owing to its quasiparticle excitations that behave like massless Dirac fermions in two spatial dimensions. This unique feature has rendered graphene a fertile ground for the application of concepts from relativistic quantum field theory (QFT) to condensed matter physics [1,2]. The Dirac-like linear dispersion near the Fermi points allows for the modeling of graphene's low-energy physics using effective Dirac equations, thereby bridging two traditionally distinct domains: high-energy physics and solid-state theory.

However, real-world graphene is not perfectly flat. Experimental observations have shown that graphene sheets naturally exhibit ripples, curvature, strain, and defects, all of which can locally modify its electronic and thermal behavior [3,4]. Theoretical studies have approached these features by embedding the effective Dirac theory of graphene into curved spacetimes, leading to an emergent field known as "graphene in curved space". In this framework, deformations such as strain and curvature are encoded as effective geometrical fields, and the Dirac equation is generalized to include the effects of a curved metric and spin connections [5,6].

Among the possible curved backgrounds, Anti-de Sitter (AdS) space has emerged as a particularly compelling geometry. Its negative curvature, maximal symmetry, and role in the AdS/CFT correspondence make it an ideal playground for studying strongly coupled systems and thermodynamic stability. The AdS/CMT program—an offshoot of the AdS/CFT duality—has suggested deep connections between gravitational backgrounds and condensed matter phenomena, including transport, superconductivity, and quantum phase transitions [7,8]. While this framework has been extensively used to model phenomena like holographic superconductors and strange metals, its application to graphene-like systems, particularly from a thermal perspective, remains underexplored.

Several studies have taken initial steps in this direction. For instance, Cortijo and Vozmediano [5] investigated the role of topological defects and local curvature on graphene's electronic structure using effective field theory methods. Cotaescu and Sporea [9] later extended this by comparing Dirac fields in de Sitter and Anti-de Sitter geometries, showing how curvature modifies fermionic

dynamics. Moreover, studies such as Furtado et al. [10] analyzed Landau levels in strained graphene using topological and geometric tools. These works, while crucial, have primarily focused on electronic properties, with limited treatment of the thermodynamic sector, particularly in curved or deformed spaces.

This gap motivates the present study, which aims to theoretically investigate the thermodynamics of graphene-like Dirac fermions in AdS space, with an emphasis on understanding how geometric curvature and interaction strength affect thermal quantities such as the partition function, free energy, entropy, internal energy, and heat capacity.

The main motivation to involve into the study is that we would;

1. **Modelling Realistic Graphene Systems**: Graphene is rarely flat in practical applications. Curvature, strain, and topological defects are inevitable. Embedding its physics in curved spacetime allows for a more accurate and geometrically consistent theoretical description.
2. **Exploring Gravitational Analogues**: The effective Dirac behaviour of electrons in graphene makes it a unique tabletop system to study analogues of gravitational and quantum field theory phenomena—especially in AdS backgrounds, which are central to modern holographic theories.
3. **Understanding Thermal Stability**: Thermal observables like entropy and heat capacity are not only crucial for applications (e.g., thermal management in graphene devices) but also for identifying signatures of instability, phase transitions, or nontrivial curvature effects.
4. **Bridging AdS/CMT and Dirac Materials**: While AdS/CMT has matured as a tool in strongly correlated systems, its direct application to thermally analysing Dirac materials in curved backgrounds is novel and holds the potential for unifying themes between high-energy and condensed matter theory.

The primary goal of this work is to perform a detailed analytical and numerical investigation of the thermodynamic behaviour of graphene-like systems modelled by Dirac fields in Anti-de Sitter (AdS) geometry. Specifically, the objectives are:

1. **To derive closed-form expressions** for the partition function of the Dirac field in AdS background, incorporating curvature and a phenomenological interaction parameter λ.

2. **To compute fundamental thermal quantities**, including free energy, internal energy, entropy, and heat capacity, and analyse their behaviour over a range of temperatures and coupling strengths.
3. **To examine the effects of spacetime curvature** (parameterized by $\tau=\pm1$ for positive/negative AdS-type curvature) on the thermal response of the system, identifying curvature-induced instabilities or critical behaviour.
4. **To determine the role of interaction strength** λ in driving thermal transitions or divergences, and to explore how it interacts with curvature in shaping the system's thermodynamic stability.
5. **To draw physical insights** relevant to both high-energy analogies (e.g., AdS/CFT thermodynamics) and practical graphene-based systems subject to deformation or strain.

Chapter 1 Generalities on Graphene and the thermodynamic Properties

1.1 Introduction

Graphene is a single-atom-thick, two-dimensional sheet of carbon atoms arranged in a hexagonal honeycomb structure. This crystalline lattice represents the foundational unit of various carbon allotropes, including graphite, carbon nanotubes, and fullerenes [11]. Each carbon atom in the lattice engages in robust covalent bonding with three adjacent atoms via sp^2 hybrid orbitals, establishing a bond length close to 0.142 nanometers.

Though theorized for more than six decades, it wasn't until 2004 that graphene was successfully isolated through mechanical exfoliation of graphite by Geim and Novoselov [12]. Their breakthrough reshaped the landscape of condensed matter physics, driven by graphene's extraordinary combination of mechanical strength, thermal conductivity, and electronic performance. These features—such as its remarkable carrier mobility exceeding 15,000 $cm^2/V \cdot s$, visibility of the quantum Hall effect even at ambient temperature, adjustable band gap, and high optical transparency—position it as a leading material for next-generation technologies including solar cells, MOSFETs, and bendable electronics [13,14].

The ability to experimentally obtain monolayer graphene marked a turning point, catalyzing the exploration of other 2D materials and broadening horizons in nanotechnology and theoretical physics alike [15].

1.2 Crystal Structure of Graphene

Graphene consists of a single atomic layer of carbon atoms arranged in a hexagonal, honeycomb-like lattice. Its unit cell contains two distinct atoms, typically labeled A and B, which differ in their lattice positions and are key to graphene's unique electronic behavior. Each carbon atom forms covalent bonds with three neighboring atoms via sp^2 hybridization, creating in-plane σ bonds with a bond length of 1.42 Å. In multilayer forms like graphite, these layers are loosely bound by van der Waals forces, maintaining an interlayer distance of roughly 3.35 Å [16].

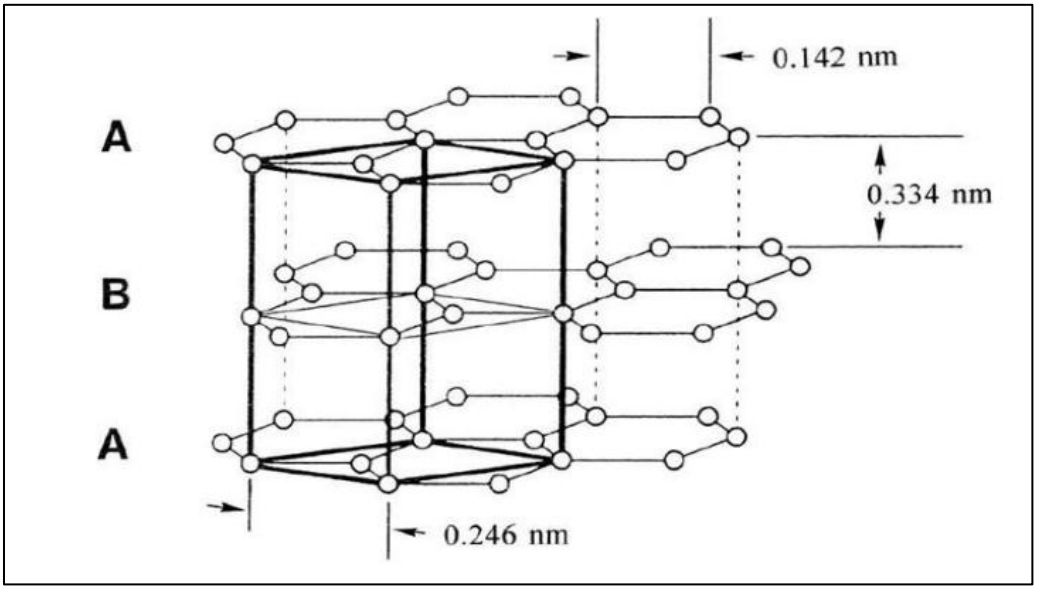

Figure 1-1. Atomic Structure of a Trilayer Graphene Arrangement.

1.3 Electronic Band Structure

In monolayer graphene, π bonds emerge from the overlap of unhybridized pz orbitals oriented perpendicular to the atomic plane. These orbitals generate the π and π* electronic bands, which intersect at specific points in the Brillouin zone known as Dirac points. Near these points, the energy-momentum relationship is linear, causing charge carriers to mimic massless Dirac fermions [17].

As a result, graphene behaves as a zero-bandgap semiconductor, or semimetal. While this characteristic enables exceptionally high electron mobility, it presents challenges for technologies that require a finite bandgap, such as digital logic circuits. In contrast, bilayer and trilayer graphene can exhibit a tunable bandgap when subjected to a perpendicular electric field, with the outcome dependent on the stacking order—Bernal or rhombohedral [18,19].

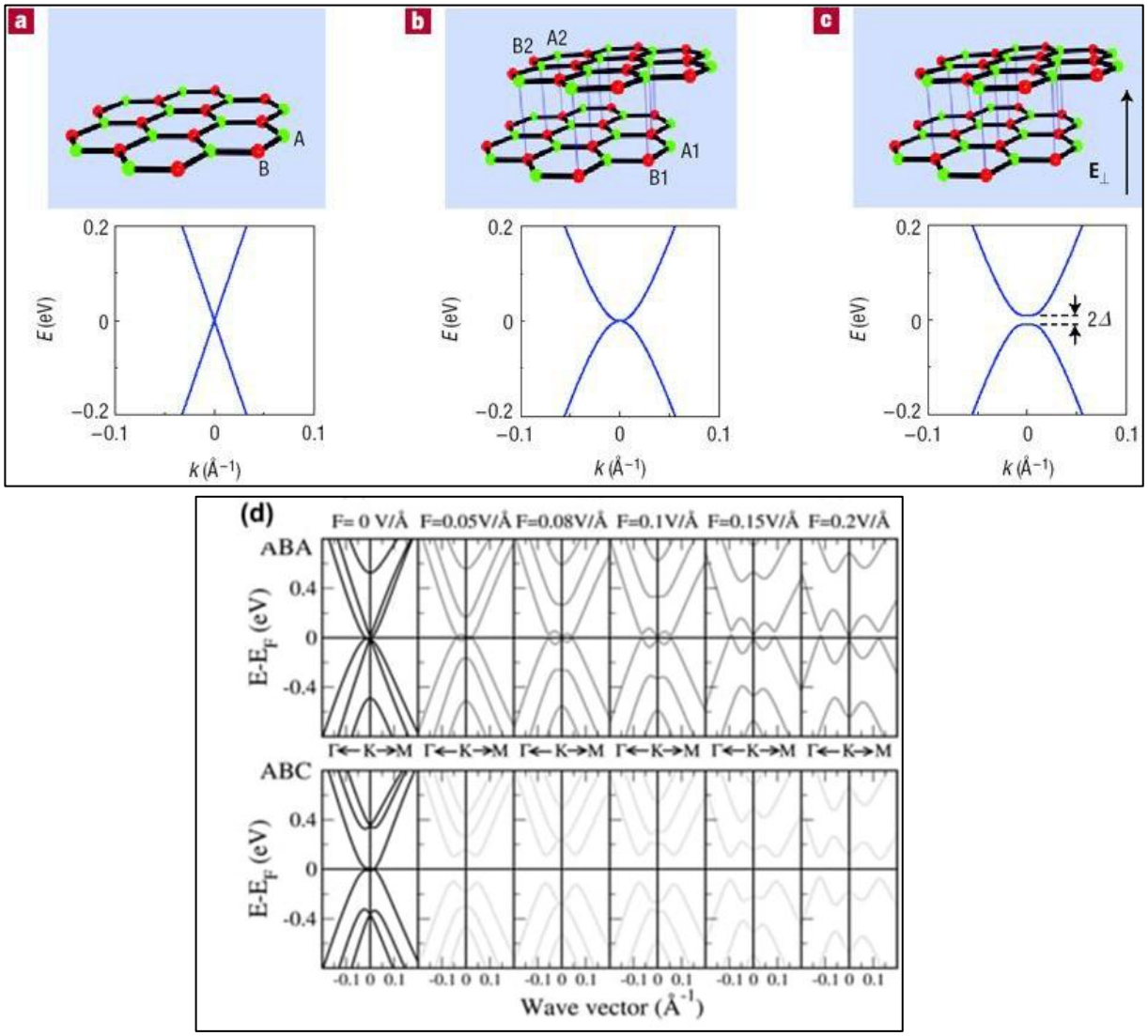

Figure 1.2. Electronic band structure of: (a) monolayer graphene (SLG), (b) bilayer graphene (BLG) without an electric field, (c) bilayer graphene (BLG) under a perpendicular electric field, and (d) trilayer graphene (TLG) with ABA and ABC stacking under the influence of an electric field.

1.4 Thermal Conductivity

Graphene demonstrates exceptionally high thermal conductivity, measured between 4800 and 5300 W/m·K at room temperature for suspended samples—far surpassing that of bulk graphite, which averages around 2000 W/m·K [20]. In contrast, supported or CVD-grown graphene shows moderately lower values due to increased phonon scattering at defects and the substrate interface [21].

Thermal transport in graphene is primarily governed by phonons, and the conductivity varies with the number of layers due to enhanced phonon-phonon Umklapp scattering effects [22].

1.5 Optical Properties

Despite being only one atom thick, graphene absorbs about 2.3% of incident white light per monolayer—a remarkably high value given its minimal thickness [23]. This absorption remains nearly uniform across a broad spectral range, a result of the material's linear band structure near the Dirac points. Graphene's optical activity spans ultraviolet, visible, and infrared wavelengths, lending it strong potential for use in photodetectors and optical modulators [24].

Moreover, its optical conductivity and refractive index can be dynamically tuned via electrostatic gating. Experiments have measured refractive indices like n = 2.0 + 1.1i in the visible spectrum for monolayer graphene placed on SiO_2 substrates [25].

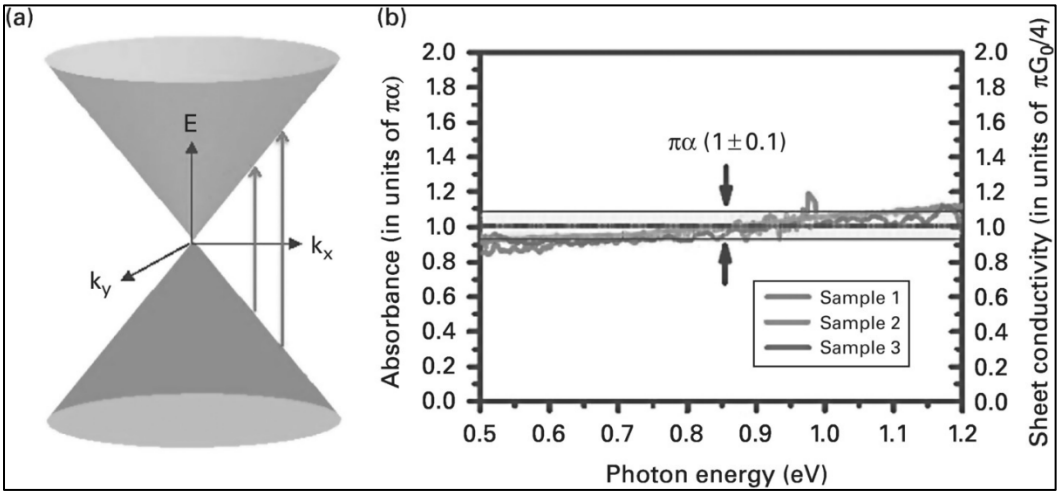

Figure 1-3. Optical Properties of Graphene - 2D Material.

1.6 Mechanical Properties

Graphene ranks among the strongest materials known to science. Atomic force microscopy (AFM) nanoindentation tests have shown that suspended monolayer graphene exhibits a Young's modulus of approximately 1 TPa and an intrinsic strength near 130 GPa [27]. These exceptional mechanical properties make it an excellent candidate for use in flexible, high-strength nanocomposites.

1.7 Graphene Types and Comparison

Graphene is found in several structural variations:

- Monolayer Graphene (SLG)
- Bilayer Graphene (BLG)

- Few-Layer Graphene (FLG)
- Graphene Oxide (GO)
- Reduced Graphene Oxide (rGO)

Each form exhibits unique electrical, thermal, and optical characteristics, driven by differences in interlayer coupling, functionalization, and defect concentrations [28].

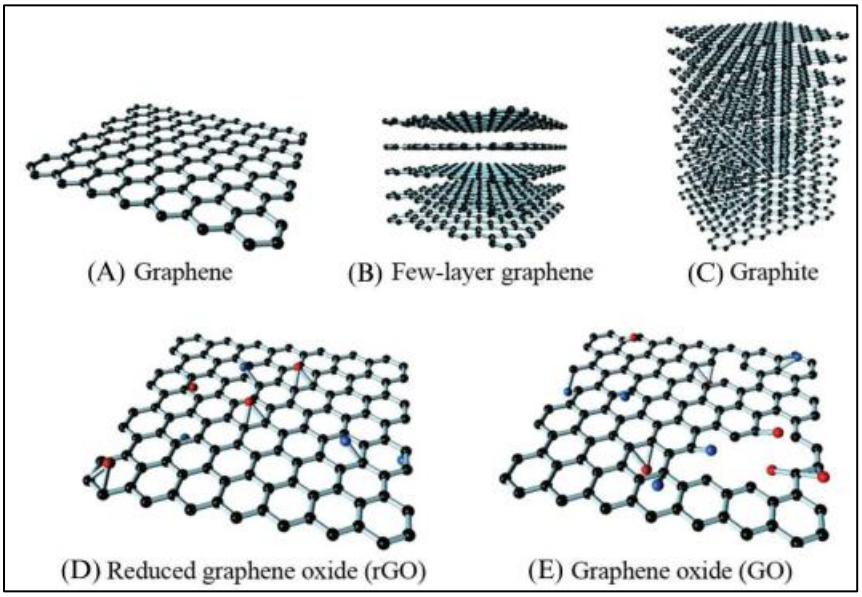

Figure 1.4. Main types of graphene family nanomaterials including A) graphene, B) few-layered graphene, C) graphite, D) reduced graphene oxide, and E) graphene oxide. Reproduced with permission.[29]

1.8 Theoretical Framework: Anti-de Sitter Space (AdS)

Anti-de Sitter (AdS) space is a solution to Einstein's field equations characterized by maximal symmetry and constant negative curvature, arising when the cosmological constant is negative. Unlike flat Minkowski spacetime, AdS space features hyperbolic geometry and plays a central role in string theory, quantum gravity, and condensed matter physics—especially through the AdS/CFT correspondence [30].

The curvature of AdS space is set by the AdS radius RAdSRAdS, and the corresponding cosmological constant is expressed as:

$$\Lambda = -\frac{(d-1)(d-2)}{2R_{AdS}^2} \qquad (1.1)$$

Here, *d* denotes the number of spacetime dimensions.

In the framework of quantum mechanics, the curvature inherent to AdS space modifies the standard canonical commutation relations, giving rise to the so-called extended uncertainty principle (EUP) [31]. These modifications are typically expressed as:

$$\left[x_i, p_j\right] = i\hbar\left(\delta_{ij} - \alpha L_{ij}\right) \text{ or } \left[x_i, p_j\right] = i\hbar\left(\delta_{ij} - \beta p^2 \delta_{ij}\right) \qquad (1.2)$$

Here, α and β represent deformation parameters, while L_{ij} denotes the angular momentum operator. These modified relations imply a fundamental lower bound on momentum uncertainty, a feature particularly relevant in quantum physics at high energies or within curved spacetimes [32,33].

1.8.1 Relevance to This Study

This study utilizes the Anti-de Sitter (AdS) framework to investigate quantum systems—particularly graphene-inspired models—within a non-Euclidean geometric setting. This approach facilitates:

- Analysis of the influence of spatial curvature on energy levels and wavefunctions,
- Integration of quantum gravitational effects via deformed commutation rules,
- Exploration of minimal length phenomena relevant near the Planck scale.

By embedding these systems in AdS geometry, we examine how physical observables in two-dimensional materials respond to curvature, revealing potential deviations from standard quantum mechanical behavior.

1.9 Thermodynamic Properties of Graphene

Graphene's thermodynamic properties stem from its distinctive two-dimensional lattice and the linear electronic dispersion near the Dirac points. In contrast to traditional semiconductors with parabolic bands, the presence of massless fermionic excitations and relativistic-like charge carriers in graphene markedly influences its heat capacity, entropy, and thermoelectric behavior.

1.9.1 Specific Heat

Graphene's specific heat reveals distinct characteristics across different temperature ranges. At low temperatures ($T < 100$ K), the linear dispersion of Dirac fermions leads to an electronic specific heat scaling as $C_e \propto T^2$ [34], contrasting with the linear $C_e \propto T$ behavior found in ordinary metals. At elevated temperatures, phonons dominate the thermal response, and the specific heat of multilayer or substrate-supported graphene trends toward the Dulong–Petit limit.

Both theory and experiment indicate that monolayer graphene's specific heat arises from a combination of acoustic phonons and the π-electron system, with anharmonic effects and phonon softening playing a significant role [35].

1.9.2 Entropy and Thermodynamic Potentials

Graphene's entropy captures its underlying quantum-statistical nature and can be formulated starting from the grand canonical potential:

$$S = -\left(\frac{\partial \Omega}{\partial T}\right)_{\mu,V} \tag{1.3}$$

Here, Ω represents the grand potential, T denotes temperature, and μ is the chemical potential. Close to the charge neutrality point—the Dirac point—entropy reaches its maximum, driven by a high density of thermally generated electron-hole pairs [36].

Thermodynamic quantities, including entropy, are highly responsive to external influences such as chemical doping, magnetic fields, or an induced bandgap. In bilayer graphene, the presence of a controllable gap enables entropy modulation, a feature of considerable importance in thermoelectric device applications [37].

1.9.3 Carrier Contributions to Thermodynamic Quantities

Owing to the linear band dispersion near the Dirac points, the density of states D(E) in graphene scales linearly with energy, thereby influencing all associated thermodynamic quantities:

$$D_E = \frac{2|E|}{\pi(\hbar v_F)^2} \tag{1.4}$$

This behavior indicates that thermodynamic observables—such as internal energy and pressure—exhibit scaling laws distinct from those in systems with quadratic dispersion. These quantities can be computed using the grand canonical partition function, accounting for contributions from both electron and hole excitations [38].

1.9.4 Thermoelectric Properties

Graphene also displays compelling thermoelectric behavior, with the Seebeck coefficient—or thermopower—being highly sensitive to the asymmetry between electron and hole transport. Close to the Dirac point, the thermopower reverses sign, indicating the presence of bipolar conduction [39] [40].

Current strategies to enhance graphene's thermoelectric efficiency have focused on:

- Inducing a finite bandgap, for instance in bilayer graphene
- Lowering thermal conductivity through nanostructuring techniques
- Boosting the power factor via chemical doping or substrate modifications

These approaches are designed to improve the dimensionless thermoelectric figure of merit ZT, which remains limited in pristine graphene primarily due to its inherently high thermal conductivity.

Chapter 2. Graphene in Anti-de Sitter Space

2.1 Introduction

This chapter sets out to develop a solid theoretical foundation for examining graphene systems within the context of Anti-de Sitter (AdS) space. The unique curvature and symmetry inherent to AdS geometry make it a compelling framework for exploring how spatial deformation can influence the quantum behavior of low-dimensional materials like graphene. We begin by reviewing the fundamental structural, electronic, thermal, and optical properties of graphene, establishing the baseline for our investigation. From there, we introduce the mathematical formulation of deformed commutation relations shaped by the AdS background. The chapter also presents the Nikiforov–Uvarov (NU) method, which serves as our primary analytical tool for tackling the modified quantum equations involved. Together, these elements prepare the groundwork for the chapters that follow, where we derive the system's energy spectrum and analyze its thermodynamic behavior in curved space.

2.2 Review of the deformed quantum mechanics relation

The deformed Heisenberg algebra leading to the EUP in AdS model is defined in 3D spaces by the following commutation relations [41][42]:

$$\left[X_i, X_j\right] = 0, \quad \left[P_i, P_j\right] = -i\hbar\lambda\varepsilon_{ijk}L_K, \quad \left[X_i, P_j\right] = i\hbar\left(\delta_{ij} - \lambda X_i X_j\right) \tag{2.1}$$

where λ is a small positive deformation parameter. In the sense of quantum gravity, this λ parameter is calculated as the fundamental constant associated with the scale factor of the expanding universe and it is proportional to the cosmological constant $\Gamma = -3\lambda = -3a^{-2}$ where a is the AdS radius [43].

L_k are the usual angular momentum components and they are expressed as follows:

$$L_K = \varepsilon_{ijk} X_i P_i \tag{2.2}$$

These components follow the usual momentum algebra:

$$\left[L_i, P_j\right] = i\hbar\lambda\varepsilon_{ijk}P_K, \quad \left[L_i, X_j\right] = i\hbar\lambda\varepsilon_{ijk}X_K, \quad \left[L_i, L_j\right] = i\hbar\lambda\varepsilon_{ijk}L_K \tag{2.3}$$

The AdS deformed algebra (2.1) gives rise to modified Heisenberg uncertainty relations:

$$\Delta X_i \Delta P_i \geq \frac{\hbar}{2}\left(1 + \lambda\left(\Delta X_i\right)^2\right), \tag{2.4}$$

where we have chosen the states for which $\langle X_i \rangle = 0$.

It also generates a minimum uncertainty in momentum. For simplicity, if we assume isotropic uncertainties $X_i = X$, we get

$$\left(\Delta P_i\right)_{\min} = \hbar\sqrt{\lambda}. \tag{2.5}$$

So, the noncommutative operators X_i and P_i satisfy the AdS algebra (2.1) with the rescaled uncertainty relations in position space (2.4). In what follows, we represent these operators as functions of the usual x_i and p_i operators fulfilling the ordinary canonical commutation relations in position space; this is done with the following transformations:

$$X_i = \frac{x_i}{\sqrt{1-\lambda r^2}}, \tag{2.6}$$

$$P_i = -i\hbar\sqrt{1-\lambda r^2}\,\partial x_i, \tag{2.7}$$

where the variable r varies in the domain $\left]-1/\lambda, 1/\lambda\right[$.

2.3 Nikiforov Uvarov Method

Primarily, the NU approach was built on the hypergeometric differential equation. The formulas used in the NU method reduce the second-order differential equations to the hypergeometric kind with a suitable coordinate transformation (note that $s \equiv s(x)$ and the primes denote the derivatives):

$$\psi''(s) + \frac{\tilde{\tau}(s)}{\sigma(s)}\psi'(s) + \frac{\sigma(s)}{\sigma^2(s)}\psi(s) = 0, \tag{2.8}$$

Where σ(s) and σ (s) are at most second-degree polynomials while the degree of the polynomial $\tilde{\tau}(s)$ is strictly less than 2 [44][45]. If we use the following factorization:

$$\psi(s) = \phi(s)y(s) \tag{2.9}$$

Equation (2.8) becomes [45]

$$\sigma(s)y''(s) + \tau(s)y'(s) + \Lambda y(s) = 0\ , \tag{2.10}$$

Where

$$\pi(s) = \sigma(s)\frac{d}{ds}(\ln\phi(s)) \ \text{ and } \ \tau(s)=\tilde{\tau}(s)+2\pi(s) \tag{2.11}$$

And Λ is defined by

$$\Lambda_n + n\tau' + \frac{n(n+1)}{2}\sigma'' = 0 \text{ and } n = 0,1,2,.... \qquad (2.12)$$

The energy eigenvalues of the system are determined from the equation above. To find their expressions, we have to evaluate π(s) and Λ first by identifying

$$k = \Lambda - \pi'(s) \qquad (2.13)$$

We get the solution of the quadratic equation for $\pi(s)$ which is a polynomial of s

$$\pi(s) = \left(\frac{\sigma' - \tilde{\tau}}{2}\right) \pm \sqrt{\left(\frac{\sigma' - \tilde{\tau}}{2}\right)^2 - \sigma + \sigma k} \qquad (2.14)$$

It must be noted that in the calculation of $\pi(s)$, the determination of k is the critical point and it is achieved by stating that the expression under the square root in (2.14) must be a polynomial square; this gives us a quadratic general equation for k. We use (2.11) and the Rodrigues relation to evaluate the polynomial solutions $yn(s)$:

$$y_n(s) = \frac{C_n}{\rho(s)}\frac{d^n}{ds^n}\left[\sigma^n(s)\rho(s)\right] \qquad (2.15)$$

where Cn are constants used to normalize the solutions. The weight function $\rho(s)$ meets the following relation:

$$\frac{d}{ds}\left[\sigma(s)\rho(s)\right] = \tau(s)\rho(s). \qquad (2.16)$$

This last equation refers to the classical orthogonal polynomials and we write the orthogonality relations for the polynomial solutions as follows:

$$\int_a^b y_n(s)y_m(s)\rho(s)ds = 0 \text{ if } m \neq n. \qquad (2.17)$$

2.4 Theoretical Study of Graphene in Anti de-Sitter space

Graphene in Anti-de Sitter (AdS) space provides a powerful theoretical setup to explore strongly correlated electronic behaviors. Leveraging AdS/CFT correspondence, one can probe thermal and quantum phenomena inaccessible in flat-space systems. This approach helps in understanding exotic phases, transport properties, and quantum critical points in graphene-like materials.

We consider the (2+1)-dimensional massless Dirac equation that describes the motion of electrons with Fermi velocity $V_F = (1.12 \pm 0.02)\ 10^6$ m.s^{-1} in quantum theory of graphene, the Hamiltonian is given by

$$\left(\alpha \bullet \mathrm{p}\right)\Psi(\mathrm{r}) = \frac{E}{V_F}\Psi(\mathrm{r}) \tag{2.18}$$

Where σ designates the Pauli matrices, $p = p_x\vec{i} + p_y\vec{j}$ is the momentum and the four-component spinor Ψ is of the form

$$\Psi(\vec{r}) = \begin{pmatrix} \psi_a(\vec{r}) \\ \psi_b(\vec{r}) \end{pmatrix} \tag{2.19}$$

On substitution of Ψ as given above into (2.18), we get the following equations for the two component spinors ψ_α (r) and ψ_b (r):

$$\begin{pmatrix} 0 & \vec{\sigma}\cdot\vec{p} \\ \vec{\sigma}\cdot\vec{p} & 0 \end{pmatrix}\begin{pmatrix} \psi_a \\ \psi_b \end{pmatrix} = \frac{E}{V_f}\begin{pmatrix} \psi_a \\ \psi_b \end{pmatrix} \tag{2.20}$$

This results in a system of equations:

$$\begin{cases} \vec{\sigma}\cdot\vec{p}\psi_b = \dfrac{E}{V_f}\psi_a \quad (*) \\ \vec{\sigma}\cdot\vec{p}\psi_a = \dfrac{E}{V_f}\psi_b \quad (**) \end{cases} \tag{2.21}$$

Notice that;

$$\vec{\alpha}\cdot\vec{p} = \sum_{i=1}^{2}\alpha_i p_i = \alpha_1 p_1 + \alpha_2 p_2 = \alpha_1 p_x + \alpha_2 p_y$$
$$= \begin{pmatrix} 0 & \alpha_x \\ \alpha_x & 0 \end{pmatrix}P_x + \begin{pmatrix} 0 & \alpha_y \\ \alpha_y & 0 \end{pmatrix}P_y \tag{2.22}$$

Which leads to

$$\begin{pmatrix} 0 & \alpha_x p_x + \alpha_y p_y \\ \alpha_x p_x + \alpha_y p_y & 0 \end{pmatrix} = \vec{\alpha}\cdot\vec{p} \tag{2.23}$$

These two equations can be used to eliminate ψ_b (r) in favor of ψ_a (r), so that one can have

$$\left(\vec{\alpha}\cdot\vec{p}\right)\left(\vec{\alpha}\cdot\vec{p}\right)\psi_a = \frac{E^2}{V_f^2}\psi_a \tag{2.24}$$

According to the following relations:

$$\left(\vec{\sigma}\cdot\vec{A}\right)\left(\vec{\sigma}\cdot\vec{B}\right) = \vec{A}\cdot\vec{B} + i\vec{\sigma}\cdot\left(\vec{A}\times\vec{B}\right) \tag{2.25}$$

The equation (2.24) can be written as

$$\left(\vec{\sigma}\cdot\vec{p}\right)\left(\vec{\sigma}\cdot\vec{p}\right) = \vec{p}\cdot\vec{p} + i\vec{\sigma}\cdot\left(\vec{p}\times\vec{p}\right) \tag{2.26}$$

We can make a proof for the expression stated below;

$$\begin{aligned}\left(\vec{\sigma}\cdot\vec{A}\right)\left(\vec{\sigma}\cdot\vec{B}\right) &= \left(\sigma_x A_x + \sigma_y A_y\right)\left(\sigma_x B_x + \sigma_y B_y\right) \\ &= \sigma_x^2 A_x B_x + \sigma_x\sigma_y A_x B_y + \sigma_y\sigma_x A_y B_x + \sigma_y^2 A_y B_y\end{aligned} \tag{2.27}$$

Knowing the commutation's relations

$$\sigma_i^2 = I \tag{2.28}$$

$$\sigma_i\sigma_j = -\sigma_j\sigma_i \quad \text{for } i \neq j \tag{2.29}$$

$$\sigma_i\sigma_j = \delta_{ij} I + i\varepsilon_{ijk}\sigma_k \tag{2.30}$$

Then, we can observe that it gives the first part as a scalar product

$$A_x B_x + A_y B_y + \sigma_x\sigma_y A_x B_y - \sigma_x\sigma_y A_x B_y = A_x B_x + A_y B_y \tag{2.31}$$

And for the vector product in the second term like,

$$\vec{A}\cdot\vec{B} + \sigma_x\sigma_y\left(A_x B_y - A_y B_x\right) \tag{2.32}$$

Which leads to the following expression

$$\vec{A}\cdot\vec{B} + i\sigma_z\left(\vec{A}\times\vec{B}\right)_z \tag{2.33}$$

Let's apply this relation on our system and introducing the magnetic field as a vector potential and using the AdS algebra (2.6) and (2.7) by defining the momentum in the deformed space

$$\vec{P} = \sqrt{1-\lambda r^2}\,\vec{p} - \vec{B}\times\vec{r} \tag{2.34}$$

Here B the intensity of the magnetic field and the vector product:

$$\vec{B}\times\vec{r} = \frac{B}{2}(-y, x, 0) \tag{2.35}$$

Now, let's explicit some calculations in order to comprehend the procedure;

$$\vec{P}_x = \left(\sqrt{1-\lambda r^2}\,p_x + \frac{eBy}{2\sqrt{1-\lambda r^2}}\right)\vec{i} \text{ and } \vec{P}_y = \left(\sqrt{1-\lambda r^2}\,p_y - \frac{eBx}{2\sqrt{1-\lambda r^2}}\right)\vec{j} \tag{2.36}$$

Let's begin with the scalar term

$$\vec{P}\bullet\vec{P} = P_x^2 + P_y^2 \tag{2.37}$$

Hence, we calculate the first part P_x^2

$$P_x^2 = \left(\sqrt{1-\lambda r^2}\,p_x + \frac{eBy}{2\sqrt{1-\lambda r^2}}\right)\bullet\left(\sqrt{1-\lambda r^2}\,p_x + \frac{eBy}{2\sqrt{1-\lambda r^2}}\right) \tag{2.38}$$

Starting with

$$\left(\sqrt{1-\lambda r^2}\cdot\frac{\hbar}{i}\frac{\partial}{\partial x}\right)\cdot\left(\sqrt{1-\lambda r^2}\cdot\frac{\hbar}{i}\frac{\partial}{\partial x}\right)=-\hbar^2\left[-\lambda x\frac{\partial}{\partial x}+\left(1-\lambda r^2\right)\frac{\partial^2}{\partial x^2}\right] \tag{2.39}$$

Then

$$\left(\sqrt{1-\lambda r^2}\cdot\frac{\hbar}{i}\frac{\partial}{\partial x}\right)\bullet\left(\frac{eBy}{2\sqrt{1-\lambda r^2}}\right)=\frac{\hbar}{i}\frac{eB}{2}\left[\frac{\lambda xy}{1-\lambda r^2}+y\frac{\partial}{\partial x}\right] \tag{2.40}$$

Now with

$$\left(\frac{eBy}{2\sqrt{1-\lambda r^2}}\right)\bullet\left(\sqrt{1-\lambda r^2}\cdot\frac{\hbar}{i}\frac{\partial}{\partial x}\right)=\frac{\hbar}{i}\frac{eB}{2}y\frac{\partial}{\partial x} \tag{2.41}$$

The last term gives

$$\left(\frac{eBy}{2\sqrt{1-\lambda r^2}}\right)\bullet\left(\frac{eBy}{2\sqrt{1-\lambda r^2}}\right)=\frac{e^2B^2y^2}{4\left(1-\lambda r^2\right)} \tag{2.42}$$

Let's move to the second part with P_y^2

$$P_y^2=\left(\sqrt{1-\lambda r^2}\,p_y-\frac{eBx}{2\sqrt{1-\lambda r^2}}\right)\bullet\left(\sqrt{1-\lambda r^2}\,p_y-\frac{eBx}{2\sqrt{1-\lambda r^2}}\right) \tag{2.43}$$

Commencing with

$$\left(\sqrt{1-\lambda r^2}\,p_y\right)\bullet\left(\sqrt{1-\lambda r^2}\,p_y\right)=-\hbar^2\left[-\lambda y\frac{\partial}{\partial y}+\left(1-\lambda r^2\right)\frac{\partial^2}{\partial y^2}\right] \tag{2.44}$$

And

$$\left(\sqrt{1-\lambda r^2}\,p_y\right)\bullet\left(-\frac{eBx}{2\sqrt{1-\lambda r^2}}\right)=-\frac{eB}{2}\frac{\hbar}{i}\left[\frac{\lambda xy}{1-\lambda r^2}+x\frac{\partial}{\partial y}\right] \tag{2.45}$$

The third term

$$\left(-\frac{eBx}{2\sqrt{1-\lambda r^2}}\right)\bullet\left(\sqrt{1-\lambda r^2}\,p_y\right)=-\frac{eB}{2}x\bullet p_y \tag{2.46}$$

To finalize it with

$$\left(-\frac{eBx}{2\sqrt{1-\lambda r^2}}\right)\bullet\left(-\frac{eBx}{2\sqrt{1-\lambda r^2}}\right)=\frac{e^2B^2x^2}{4\left(1-\lambda r^2\right)} \tag{2.47}$$

Now we sum all the terms together respectively to obtain the scalar part as below;

$$\begin{aligned}\vec{P}\bullet\vec{P}=P_x^2+P_y^2=i\hbar\lambda\left(\vec{r}\bullet\vec{p}\right)+\left(1-\lambda r^2\right)p^2+\frac{e^2B^2}{4}\frac{r^2}{1-\lambda r^2}\\+eB\left(yp_x-xp_y\right)\end{aligned} \tag{2.48}$$

After completing the first part which concerning the scalar product, we move to the vector one's;

$$\vec{P}\times\vec{P}=\begin{pmatrix} P_x & P_y \\ P_x & P_y \end{pmatrix}=P_xP_y-P_yP_x \tag{2.49}$$

So, let's get started with the first term

$$P_x\bullet P_y=\left(\sqrt{1-\lambda r^2}\,p_x+\frac{eBy}{2\sqrt{1-\lambda r^2}}\right)\bullet\left(\sqrt{1-\lambda r^2}\,p_y-\frac{eBx}{2\sqrt{1-\lambda r^2}}\right) \tag{2.50}$$

We do the same calculations as above, which gives

$$\left(\sqrt{1-\lambda r^2}\,p_x\right)\bullet\left(\sqrt{1-\lambda r^2}\,p_y\right)=-\hbar^2\left[-\lambda x\frac{\partial}{\partial y}+\left(1-\lambda r^2\right)\frac{\partial}{\partial x\partial y}\right] \tag{2.51}$$

The second one

$$\left(\sqrt{1-\lambda r^2}\,p_x\right)\bullet\left(-\frac{eBx}{2\sqrt{1-\lambda r^2}}\right)=-\frac{eB}{2}\frac{\hbar}{i}\left[\frac{1-\lambda r^2+\lambda x^2}{1-\lambda r^2}+x\frac{\partial}{\partial x}\right] \tag{2.52}$$

Moreover;

$$\left(\frac{eBy}{2\sqrt{1-\lambda r^2}}\right)\bullet\left(\sqrt{1-\lambda r^2}\,p_y\right)=\frac{eBy}{2}\,p_y \tag{2.53}$$

The last one gives;

$$\left(\frac{eBy}{2\sqrt{1-\lambda r^2}}\right)\bullet\left(-\frac{eBx}{2\sqrt{1-\lambda r^2}}\right)=-\frac{e^2B^2xy}{4\left(1-\lambda r^2\right)} \tag{2.54}$$

Let's continue with the second part now,

$$P_yP_x=\left(\sqrt{1-\lambda r^2}\,p_y-\frac{eBx}{2\sqrt{1-\lambda r^2}}\right)\bullet\left(\sqrt{1-\lambda r^2}\,p_x+\frac{eBy}{2\sqrt{1-\lambda r^2}}\right) \tag{2.55}$$

We evaluate the expression as we have done to get the following;

$$\left(\sqrt{1-\lambda r^2}\,p_y\right)\bullet\left(\sqrt{1-\lambda r^2}\,p_x\right)=-\hbar^2\left[-\lambda y\frac{\partial}{\partial x}+\left(1-\lambda r^2\right)\frac{\partial}{\partial x\partial y}\right] \tag{2.56}$$

Also

$$\left(\sqrt{1-\lambda r^2}\,p_y\right)\bullet\left(\frac{eBy}{2\sqrt{1-\lambda r^2}}\right)=\frac{eB}{2}\frac{\hbar}{i}\left[\frac{1-\lambda r^2+\lambda y^2}{1-\lambda r^2}+y\frac{\partial}{\partial y}\right] \tag{2.57}$$

Besides

$$\left(-\frac{eBx}{2\sqrt{1-\lambda r^2}}\right)\bullet\left(\sqrt{1-\lambda r^2}\,p_x\right)=-\frac{eBx}{2}p_x \tag{2.58}$$

To sum up with the last term;

$$\left(-\frac{eBx}{2\sqrt{1-\lambda r^2}}\right)\bullet\left(\frac{eBy}{2\sqrt{1-\lambda r^2}}\right)=-\frac{e^2B^2xy}{4\left(1-\lambda r^2\right)} \tag{2.59}$$

We can easily sum all the obtained terms of the vector product to obtain;

$$\vec{P}\times\vec{P}=i\hbar\lambda\left(\vec{r}\times\vec{p}\right)-eB\frac{\hbar}{i}-\frac{eB}{2}\frac{\hbar}{i}\lambda\frac{r^2}{1-\lambda r^2} \tag{2.60}$$

By combining the two terms of eqs (2.48) with (2.60), we can the differential equation of the graphene in the deformed space;

$$\begin{aligned}&\left[\left\{i\hbar\lambda\left(\vec{r}\bullet\vec{p}\right)+\left(1-\lambda r^2\right)p^2\right\}+\frac{e^2B^2}{4}\frac{r^2}{1-\lambda r^2}+eB\left(yp_x-xp_y\right)\right]\\&+\sigma_z\left[-\hbar\lambda\left(\vec{r}\times\vec{p}\right)-eB\hbar-\frac{eB}{2}\hbar\lambda\frac{r^2}{1-\lambda r^2}\right]\psi_a=\frac{E^2}{V_f^2}\psi_a\end{aligned} \tag{2.61}$$

Since we have the angular momentum $L_z=\vec{r}\times\vec{p}$,then we can rearrange the equation again to be like:

$$\left[(1-\lambda r^2)p^2+\eta\frac{r^2}{1-\lambda r^2}+i\hbar\lambda\left(\vec{r}\cdot\vec{p}\right)-\beta L_z-\varepsilon\right]\psi_a(\vec{r})=0 \tag{2.62}$$

Where the parameters defined as

$$\eta=\frac{e^2B^2}{4}-\frac{eB}{2}\hbar\sigma_z\lambda\ ,\ \beta=eB+\lambda\hbar\sigma_z\ \text{and}\ \varepsilon=eB\hbar\sigma_z+\frac{E^2}{V_F^2} \tag{2.63}$$

To solve the equation.(2.62), we use the following ansatz $\psi_a(\vec{r})=e^{il\varphi}R_{nl}(r)\chi_\tau$, where n is the radial quantum number, l and τ=±1 are, respectively, the eigenvalues of angular momentum and spin operators, and $\chi_{+1}^T=(1,0),\quad \chi_{-1}^T=(0,1)$ are the spin functions.

Using the polar coordinates of the position and momentum operators, we obtain the following differential equation for the radial part of the wave function:

$$\left[\left(\sqrt{1-\lambda r^2}\frac{d}{dr}\right)^2-\frac{l^2(1-\lambda r^2)}{r^2}-\frac{\eta^\tau r^2}{\hbar^2(1-\lambda r^2)}+\varepsilon^\tau\right]R_{nl}(r)=0 \tag{2.64}$$

With

$$\eta^{\tau}=\frac{e^2B^2}{4}-\frac{eB}{2}\lambda\hbar\tau \text{ and } \varepsilon^{\tau}=\frac{\varepsilon}{\hbar^2}+\frac{l}{\hbar}\left(eB+\lambda\hbar\tau\right) \tag{2.65}$$

Now to solve eq. (2.64), we use the following transformation:

$$\rho=\sqrt{1-\lambda r^2},\quad R(\rho)=\rho^{\mu}g(\rho) \tag{2.66}$$

with

$$\begin{aligned}\frac{d}{d\rho}R(\rho)&=\rho^{\mu}\left(\frac{d}{d\rho}+\frac{\mu}{\rho}\right)g(\rho)\\ \frac{d^2}{d\rho^2}R(\rho)&=\rho^{\mu}\left(\frac{d^2}{d\rho^2}+\frac{2\mu}{\rho}\frac{d}{d\rho}+\frac{\mu(\mu-1)}{\rho^2}\right)g(\rho)\end{aligned} \tag{2.67}$$

By replacing the eq. (2.67) into eq. (2.64), it gives us

$$\left[(1-\rho^2)\frac{d^2}{d\rho^2}+2\left(\frac{\mu}{\rho}-(\mu+1)\rho\right)\frac{d}{d\rho}-\frac{l^2\rho^2}{1-\rho^2}+\varepsilon'\right]g(\rho)=0 \tag{2.68}$$

Where

$$\varepsilon'=\frac{1}{\lambda}\left(\frac{\varepsilon}{\hbar^2}+\frac{eBl}{\hbar}\right)-2\mu \tag{2.69}$$

where we have chosen the free parameter μ so that it satisfies the relation:

$$\mu(\mu-1)-\frac{\eta}{\hbar^2\lambda^2}=0 \tag{2.70}$$

The solutions of this equation are given by:

$$\mu=\frac{1}{2}\pm\sqrt{\frac{1}{4}+\frac{\eta}{\hbar^2\lambda^2}} \tag{2.71}$$

From eq. (2.68), we see that g(ρ) should be nonsingular at ρ=±1 and the same is true for R(ρ) from eq. (2.66); thus, the accepted value of μ is:

$$\mu=\frac{1}{2}+\sqrt{\frac{1}{4}+\frac{\eta}{\hbar^2\lambda^2}} \tag{2.72}$$

We note that eq. (2.68) possesses three singular points ρ=0,1, -1 and to reduce it to a class of known differential equation with a polynomial solution, we use another change of variable $s=2\rho^2-1$, with

$$\begin{aligned}\frac{ds}{d\rho}=4\rho\Rightarrow\quad \frac{d}{d\rho}&=4\rho\frac{d}{ds},\\ \frac{d^2}{d\rho^2}&=16\rho^2\frac{d^2}{ds^2}+4\frac{d}{ds}\end{aligned} \tag{2.73}$$

replacing eq (2.73) into eq (2.68), we get;

$$\left[\frac{d^2}{ds^2}+\frac{(\mu-\frac{1}{2})-(\mu+\frac{3}{2})s}{1-s^2}\frac{d}{ds}-\frac{(l^2+\varepsilon^{'})s^2+2l^2s-(\varepsilon^{'}-l^2)}{4(1-s^2)^2}\right]g(s)=0 \qquad (2.74)$$

Comparing eq. (2.74) with eq. (2.8) allows us to use the NU method with polynomials given by:

$$\begin{aligned}&\sigma(s)=1-s^2,\quad \tilde{\sigma}(s)=\frac{1}{4}\left[-(l^2+\varepsilon^{'})s^2-2l^2s+(\varepsilon^{'}-l^2)\right],\\&\tilde{\tau}(s)=\mu-\frac{1}{2}-(\mu+\frac{3}{2})s\end{aligned} \qquad (2.75)$$

We replace them in eq. (2.14) to get:

$$\pi(s)=\frac{(\mu-\frac{1}{2})(s-1)}{2}\pm\sqrt{\frac{1}{2}\left((\mu-\frac{1}{2})^2+l^2-(4k-\varepsilon^{'})\right)s^2-\left((\mu-\frac{1}{2})^2-l^2\right)s+\frac{1}{2}\left((\mu-\frac{1}{2})^2+l^2+(4k-\varepsilon^{'})\right)} \qquad (2.76)$$

The parameter k is determined as mentioned in the precedent section and we get two values:

$$k_1=\frac{\varepsilon^{'}}{4}+\frac{l}{2}(\mu-\frac{1}{2}),\quad k_2=\frac{\varepsilon^{'}}{4}-\frac{l}{2}(\mu-\frac{1}{2}) \qquad (2.77)$$

For π(s), we obtain the following solutions:

$$\pi(s)=\begin{cases}\pi_{1,3}=\frac{1}{2}\left[(2\mu\mp l+1)s-(2\mu\pm l-1)\right]\\ \pi_{2,4}=\pm\frac{l}{2}(s+1)\end{cases} \qquad (2.78)$$

where π_1 and π_2 are related to k_1 while π_3 and π_4 are linked to k_2.

In our case, the relevant solution is the proper value π_4, so that we have:

$$\tau(s)=-(\mu+\frac{3}{2}+l)s+(\mu-\frac{1}{2}-l) \qquad (2.79)$$

From eqs. (2.12) and (2.13), we obtain:

$$\Lambda_n=k_2-\frac{l}{2}=n\left(n+\mu+l+\frac{1}{2}\right),\quad n=0,1,2,\ldots \qquad (2.80)$$

Hence, we found the expressions of the energy eigenvalues as:

$$E^{\lambda}_{n,l,\tau}=\pm\frac{\hbar V_F}{l_B}\left[(2n+l+1)\sqrt{1-2\lambda l_B^2\tau+\lambda^2 l_B^4}+\lambda l_B^2\left(4n(n+l+1)+(2-\tau)l+1\right)-(l+\tau)\right]^{1/2} \qquad (2.81)$$

where $l_B = \sqrt{\frac{\hbar}{eB}}$ is the fundamental length scale in the presence of a magnetic field.

And here by replacing τ=±1, we get:

$$E^{\lambda}_{n,l,+1} = \pm \frac{\hbar V_F}{l_B} \sqrt{2n\left(1+\lambda l_B^2(2n+2l+1)\right)}$$
$$E^{\lambda}_{n,l,-1} = \pm \frac{\hbar V_F}{l_B} \sqrt{2(n+1)\left(1+\lambda l_B^2(2n+2l+1)\right)} \quad (2.82)$$

To deduce the complete expression of the wave functions R(r), we use the relations of $\pi_4(s)$ as follows. We first get

$$\pi(s) = \pi_4(s) = \sigma(s)\frac{d}{ds}\ln\phi(s) \quad \Rightarrow \quad \phi(s) = \exp\left(\int \frac{\pi(s)}{\sigma(s)} ds\right) \quad (2.83)$$

After the calculation of the integral we obtain the function φ(s) as

$$\phi(s) = (1-s)^{l/2} \quad (2.84)$$

We use (2.16) to find the weight function ρ(s)

$$\frac{d}{ds}\left[\sigma(s)\rho(s)\right] = \tau(s)\rho(s) \quad \Rightarrow \quad \int \frac{d\rho(s)}{\rho(s)} = \int\left(\frac{\tau(s)}{\sigma(s)} - \frac{d\sigma(s)/ds}{\sigma(s)}\right) ds \quad (2.85)$$

When we compute the integral, we get

$$\ln\rho(s) = \int\left(\frac{\tau(s)}{\sigma(s)} - \frac{d\sigma(s)/ds}{\sigma(s)}\right) ds \quad \Rightarrow \quad \rho(s) = \exp\left[\int\left(\frac{\tau(s)}{\sigma(s)} - \frac{\sigma'(s)}{\sigma(s)}\right) ds\right] \quad (2.86)$$

We substitute by the expression of τ(s) equation (2.79) and σ(s) equation (2.75), after that we calculate the integral, we find

$$\rho(s) = (1+s)^{\mu-\frac{1}{2}}(1-s)^{l} \quad (2.87)$$

The $y_n(s)$part is given by Rodrigues relation as follows;

$$y_n(s) = \frac{C_n}{\rho(s)}\frac{d^n}{ds^n}\left[(1-s^2)^n \rho(s)\right] \quad (2.88)$$

By substituting the expression of ρ(s) from equation (<ref>2.47</ref>)

$$y_n(s) = \frac{C_n}{\rho(s)}\frac{d^n}{ds^n}\left[(1-s^2)^n (1+s)^{\mu-\frac{1}{2}}(1-s)^{l}\right] \quad (2.89)$$

We see that eq. (2.87) stands for the Jacobi polynomials:

$$y_n(s) \equiv P_n^{(l,\mu-\frac{1}{2})}(s) \quad (2.90)$$

Hence, f(s) can be written in the following form:

$$f(s) = C_n (1-s)^{l/2} P_n^{(l,\mu-\frac{1}{2})}(s) \qquad (2.91)$$

In terms of the variables r and ϕ, we can now write the general form of the wave function Ψ:

$$\Psi_n(r,\varphi) = C_n 2^{l/2} e^{il\varphi} (1-\lambda r^2)^{\mu/2} (\lambda r^2)^{l/2} P_n^{(l,\mu-\frac{1}{2})}\left(1-2\lambda r^2\right) \qquad (2.92)$$

In this chapter, we have successfully derived the exact energy spectrum and corresponding wavefunctions for a graphene-like system embedded in an Anti-de Sitter (AdS) background, characterized by a curvature parameter λ. Employing the Nikiforov–Uvarov method in conjunction with appropriate variable transformations, we solved the deformed Graphene equation under the influence of an external magnetic field. The resulting energy eigenvalues reveal the effects of both curvature and magnetic interactions, while the normalized wavefunctions were expressed in terms of Jacobi polynomials, showcasing their underlying orthogonal structure. These findings provide a robust analytic foundation for exploring quantum behaviors of relativistic systems in curved 2D geometries, with potential applications in topological materials, strained graphene, and quantum Hall systems on curved manifolds.

Chapter 3. Thermodynamic Properties

3.1 Introduction

This chapter explores the thermodynamic properties of graphene within the framework of Anti-de Sitter (AdS) spacetime, utilizing the AdS/CFT correspondence to establish a theoretical model. Graphene, a two-dimensional hexagonal lattice of carbon atoms, exhibits unique electronic and thermal characteristics, making it a prime candidate for studying quantum field theory effects and holographic duality.

We leverage the partition function formalism to derive and examine key thermodynamic quantities such as entropy, free energy, specific heat, and susceptibility. Mathematica software is employed throughout for symbolic computations and for generating clear, insightful plots that illustrate the temperature dependence and other significant aspects of graphene's thermodynamics in the AdS background.

By combining analytical approaches with computational visualization, this study aims to deepen our understanding of how quantum and relativistic effects manifest in low-dimensional materials like graphene when examined from the holographic perspective.

3.2 Thermodynamic Properties

In statistical mechanics, the partition function Z plays a central role, encapsulating the statistical characteristics of systems in thermodynamic equilibrium. It depends on temperature and other parameters such as the volume containing the gas. Essential thermodynamic variables, including total energy, free energy F, entropy S, and pressure P, can typically be expressed directly through the partition function or its derivatives.

We now shift our attention to exploring the thermodynamic behavior of the system. The partition function at finite temperature T is given by:

$$Z = \sum_{n=0}^{\infty} e^{-\frac{E_n}{K_B T}} = \sum_{n=0}^{\infty} \exp\left(-\frac{\hbar V_F}{l_B} \sqrt{a_1 + a_2 n + a_3 n^2} \right) \tag{3.1}$$

Here K_B is the Boltzmann constant and the expressions of the other parameters obtain from the energy spectrum eq. (2.81)

$$a_1 = (l+1)\sqrt{1-2\lambda l_B^2\tau+\lambda^2 l_B^4} + \lambda l_B^2\left((2-\tau)l+1\right) - (l+\tau) \tag{3.2}$$

$$a_2 = 2\left[2\lambda l_B^2(l+1) + \sqrt{1-2\lambda l_B^2\tau+\lambda^2 l_B^4}\right] \tag{3.3}$$

$$a_3 = 4\lambda l_B^2 \tag{3.4}$$

In order to evaluate this function, we use the Euler-MacLaurin formula:

$$\sum_{n=0}^{\infty} f(n) = \frac{1}{2}f(0) + \int f(x)dx - \sum_{p=1}^{\infty}\frac{B_{2p}}{(2p)!}f^{(2p-1)}(0) \tag{3.5}$$

B_{2p} are the Bernoulli numbers, $f^{(2p-1)}$ is the derivative of order (2p-1) and the integral term is given by:

$$I = \frac{2a_1}{\sqrt{a_2^2-4a_1a_3}}\sum_{n=0}^{\infty}(-1)^n\frac{(2n-1)!!}{(2n)!!}\left(\frac{4a_1a_3}{a_2^2-4a_1a_3}\right)^n\left[\frac{\Gamma(2n+2)}{\chi^{2n+2}} - \frac{e^{-\chi}}{2n+2}\Phi(1,2n+2,\chi)\right] \tag{3.6}$$

where we have used $\chi = \left(\frac{\hbar V_F}{l_B k_B T}\right)\sqrt{a_1}$, the new variable $y = \sqrt{1+\frac{a_2}{a_1}n+\frac{a_3}{a_1}n^2}$ and the power series of the square root of the integral:

$$I = \frac{2a_1}{\sqrt{a_2^2-4a_1a_3}}\int_1^{+\infty} e^{-\chi y}\left(1+\frac{4a_1a_3}{a_2^2-4a_1a_3}y^2\right)y\,dy \tag{3.7}$$

At high temperatures, we can ignore the first and the third terms in eq. (3.5) and keep only the integral. Similarly, we neglect the $e^{-\chi}$ term beside the $\chi^{-(2n+2)}$ one in eq.(3.7). Therefore, the partition function becomes:

$$Z = \left(\frac{\hbar V_F}{l_B}\right)^2\cdot\frac{2}{\sqrt{a_2^2-4a_1a_3}}\sum_{n=0}^{\infty}(-1)^n\frac{(2n-1)!!}{(2n)!!}\Gamma(2n+2)\sigma^n \tag{3.8}$$

With

$$\sigma = \left(\frac{\hbar V_F}{l_B}\right)^2\cdot\frac{4a_3}{a_2^2-4a_1a_3} \tag{3.9}$$

We restrict ourselves to the first order in λ, so we can reduce Z to the following simplified form:

$$Z = \frac{2\left(\frac{\hbar V_F}{l_B k_B T}\right)^2}{\sqrt{4(1+\lambda l_b^2\tau)^2}}\left[1-\frac{12(4\lambda l_B^2)kTl_B}{\hbar V_F\cdot 4(1+\lambda l_B^2\tau)^2}\right] \tag{3.10}$$

The first term is the usual partition function for a 2D scalar Graphene with a uniform magnetic field in the r-representation. The second term expresses the contribution that comes from the space deformation through the AdS algebra.

At this stage, we can evaluate all the thermodynamic properties of our system (free energy F, mean energy U, specific heat C and entropy S) using their definitions [46]:

$$F = -k_B T \ln Z,\ U = k_B T^2 \frac{\partial \ln Z}{\partial T},\ C = \frac{\partial U}{\partial T},\ S = -\frac{\partial F}{\partial T} \qquad (3.11)$$

we utilize Mathematica software to analyze and visualize the thermodynamic properties of the system. By implementing symbolic and numerical computations, we compute key quantities such as the free energy, internal energy, entropy, and heat capacity as functions of temperature and system parameters. The flexibility of Mathematica allows us to explore their behavior under various physical conditions and to generate precise plots that illustrate the thermal response of the model.

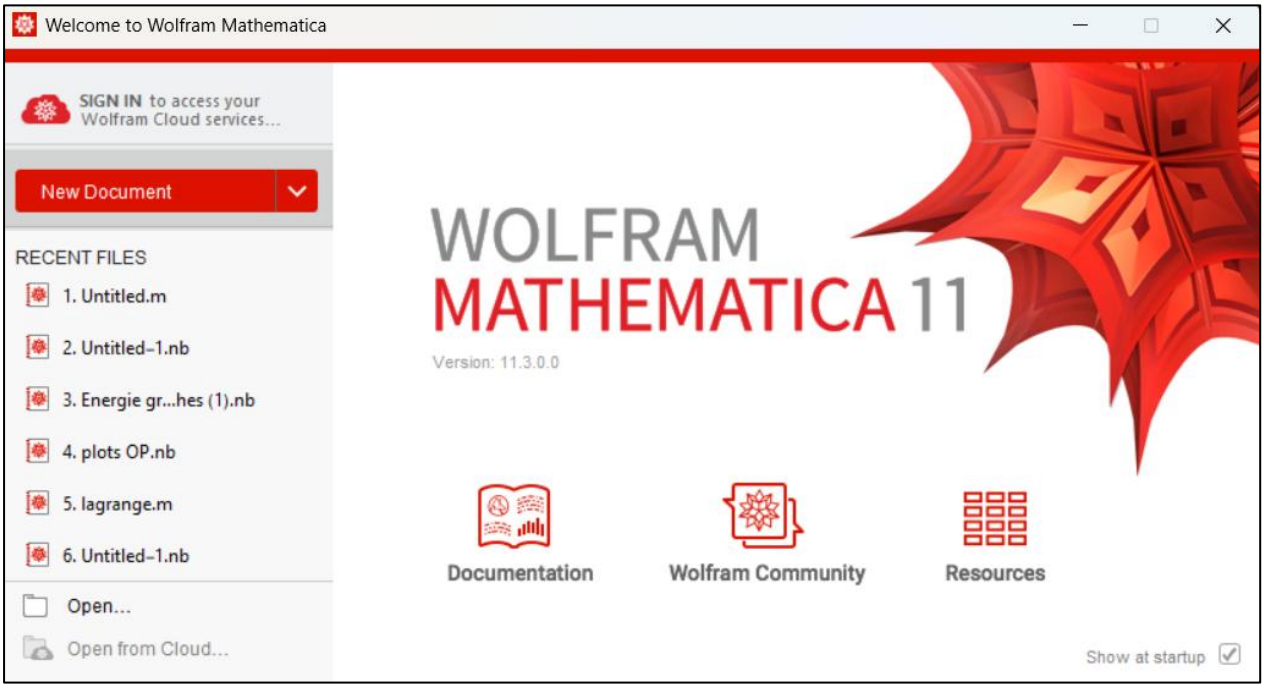

Figure 3-1. Wolfram Mathematica 11 Startup Interface

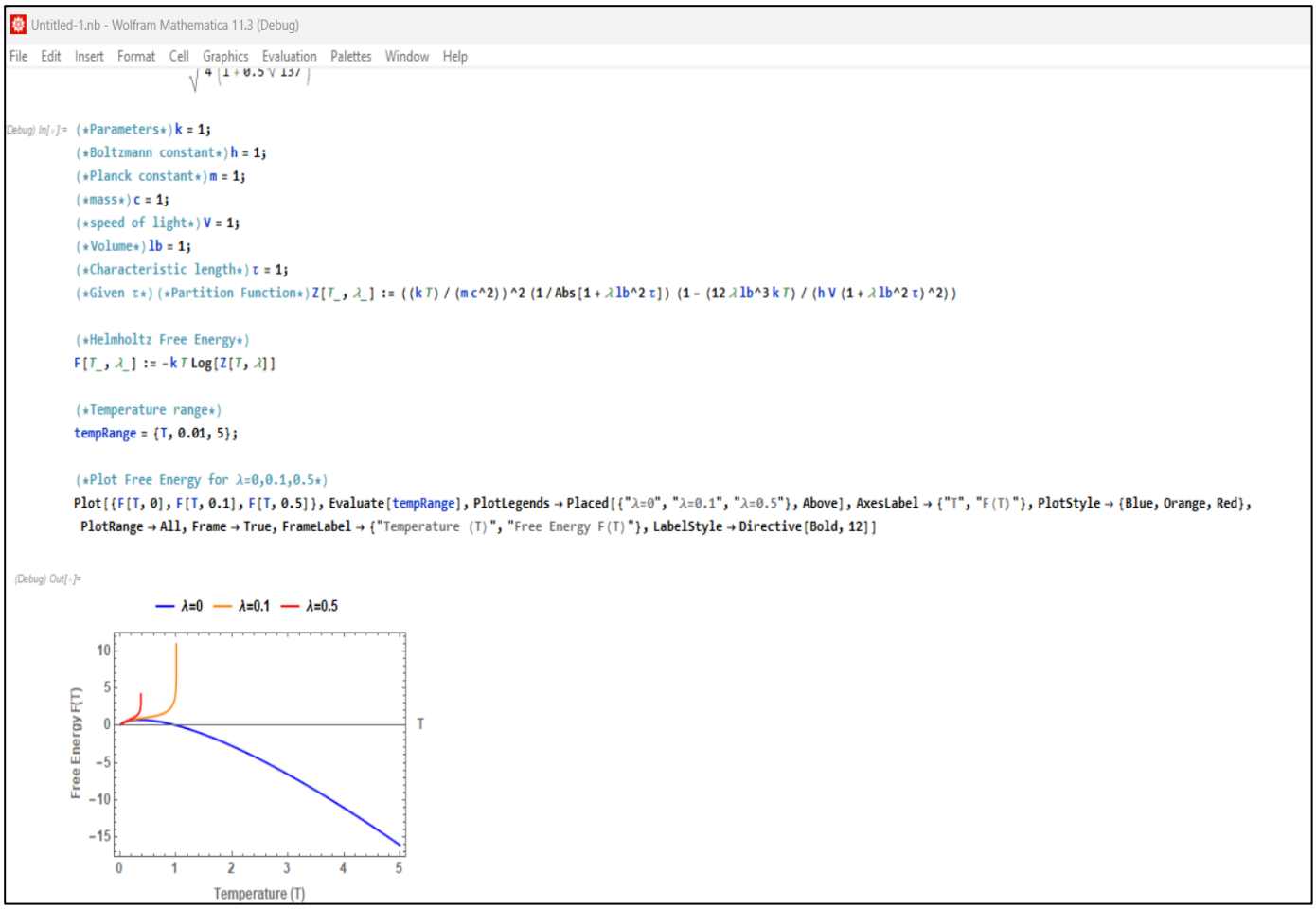

Figure 3-2: Implementation of Free Energy Calculation in AdS Space Using Wolfram Mathematica.

This is the code for plotting the free energy F as a function of temperature T

(*Parameters*)$k = 1$; (*Boltzmannconstant*)$hbar = 1$; (*reducedPlanckconstant*)m
$= 1$; (*mass*)$c = 1$; (*speedoflight*)$V = 1$; (*Volume*)lB = 1; (*Characteristiclength*)τ
$= 1$; (*Givenτ*)(*PartitionFunction*)Z[T_, λ_]:
$= (((hbar\ V\_F\ ))\ /\ ((l\_B\ )))$^2(1/Abs[1 + λlb^2$\tau$])(1
$-$ (12λlb^3kT)/($hbarV\_F$(1 + λlb^2τ)^2))□(*HelmholtzFreeEnergy*)□F[T_, λ_]:
$= -kT$Log[$Z[T, \lambda]$]]□(*Temperaturerange*)□tempRange
$= \{T, 0.01,5\}$; □(*PlotFreeEnergyforλ
$= 0,0.1,0.5$*)□Plot[{$F[T, 0], F[T, 0.1], F[T, 0.5]$}, Evaluate[tempRange], PlotLegends
→ Placed[{"λ = 0", "λ = 0.1", "λ = 0.5"}, Above], AxesLabel → {"T", "F(T)"}, PlotStyle
→ {Blue, Orange, Red}, PlotRange → All, Frame → True, FrameLabel
→ {"Temperature (T)", "Free Energy F(T)"}, LabelStyle → Directive[Bold, 12]]

For the mean energy U

(*Parameters*)$k = 1; hbar = 1; m = 1; c = 1; V\_F = 1$; l_B = 1; τ
$= -1$; □(*Partitionfunction*)□Z[T_, λ_]
≔ ($(hbar\ V_F)/(l_B)$)^2(1/Abs[1 + λl_B$^{2\tau}$])(1
$-$ (12λl_B^{3kT})/($hbarV_F(1 + \lambda$l_B$^{2\tau})^2$)); □(*InternalEnergy*)□U[T_, λ_]
≔ $kT^{2}D$[Log[Z[TT, λ]], TT]/. TT → T; □(*Temperaturerange*)□tempRange
$= \{T, 0.01,5\}$; □(*PlotInternalEnergy*)□Plot[{$U[T, 0], U[T, 0.1], U[T, 0.5]$}, Evaluate[tempRange],
PlotLegends → Placed[{"λ = 0", "λ = 0.1", "λ = 0.5"}, Above], AxesLabel
→ {"T", "Internal Energy U(T)"}, PlotStyle → {Blue, Orange, Red}, PlotRange
→ All, Frame → True, FrameLabel
→ {"Temperature (T)", "Internal Energy U(T)"}, LabelStyle
→ Directive[Bold, 12], ImageSize → Large, PlotPoints → 200, MaxRecursion
→ 4]

We can also plot the capacity heat C by using the following code

(*Parameters*)$k = 1; hbar = 1; m = 1; c = 1; V\_F = 1;$ l_B $= 1; \tau$
$= 1;$ (*Partitionfunction*)Z[T_, λ_]
$:=$ (((*hbar V_F*)) / ((*l_B*))^2(1/Abs[1 + $\lambda l_F^{2\tau}$])(1
$- (12\lambda l_B^3 kT)/\left(hbar V_{F(1+\lambda l_B^{2\tau})}^2\right)$); (*InternalEnergy*)$U$[T_, λ_]
$:= kT^{2}D$[Log[Z[TT, λ]], TT]/. TT → T; □(*HeatCapacityC_V*)Cv[T_, λ_]
$:= D[U$[TT, λ], TT]/. TT → T; (*Temperaturerange*)tempRange
$= \{T, 0.01,5\}$; (*PlotHeatCapacity*)Plot[{Cv[T, 0], Cv[T, 0.1], Cv[T, 0.5]},
Evaluate[tempRange], PlotLegends → Placed[{"λ = 0", "λ = 0.1", "λ
= 0.5"}, Above], AxesLabel → {"T", "Heat Capacity C_V(T)"}, PlotStyle
→ {Blue, Orange, Red}, PlotRange → All, Frame → True, FrameLabel
→ {"Temperature (T)", "Heat Capacity C_V(T)"}, LabelStyle
→ Directive[Bold, 12], ImageSize → Large, PlotPoints → 200, MaxRecursion
→ 4]

Also, we can evaluate the entropy as a function of T

(*Parameters*)$k = 1; hbar = 1; m = 1; c = 1; V\_F = 1;$ l_B $= 1; \tau$
$= 1;$ (*Partitionfunction*)Z[T_, λ_]:
$=$ ((*hbar V_F*)) / ((*l_B*))^2(1/Abs[1 + λl_B^2τ])(1
$-$ (12λl_B^3kT)/(*hbar*$V_F(1 + \lambda$l_B^2τ)^2)); (*InternalEnergy*)□U[T_, λ_]:
$= kT^{2}D$[Log[Z[TT, λ]], TT]/. TT → T; (*Entropy*)S[T_, λ_]:
$= k$Log[$Z[T, \lambda]] + U[T, \lambda]/T$; (*Temperaturerange*)tempRange
$= \{T, 0.01,5\}$; (*PlotEntropy*)Plot[{$S[T, 0], S[T, 0.1], S[T, 0.5]$}, Evaluate[tempRange], PlotLegends
→ Placed[{"λ = 0", "λ = 0.1", "λ = 0.5"}, Above], AxesLabel
→ {"T", "Entropy S(T)"}, PlotStyle → {Blue, Orange, Red}, PlotRange → All, Frame
→ True, FrameLabel → {"Temperature (T)", "Entropy S(T)"}, LabelStyle
→ Directive[Bold, 12], ImageSize → Large, PlotPoints → 200, MaxRecursion → 4]

The upcoming chapter presents a detailed discussion of the obtained results alongside the corresponding plots. It analyses the behaviour of the thermodynamic quantities under different parameter values and highlights the physical implications of the model. Graphical representations are used to support the interpretation and provide clear insights into the system's thermal response.

Chapter 4. Results and Discussion

4.1 Introduction

In this chapter, we present the results concerning the energy spectrum and wave function of graphene embedded in Anti-de Sitter (AdS) space. The analysis reveals how the curvature of the background geometry influences the quantum states of the system. In addition, we examine the thermal behavior of graphene by evaluating key thermodynamic quantities such as free energy, internal energy, entropy, and heat capacity. These properties are plotted as functions of temperature and system parameters, providing a comprehensive view of how curvature and coupling constants affect the physical behavior of the material

4.2 Energy eigenvalues of graphene

According to the spectrum of the graphene in the studied space eq (2.81), The energy spectrum derived for graphene in an Anti-de Sitter (AdS) background reflects how the curvature of spacetime and external parameters significantly modify the relativistic Landau levels. The presence of the AdS curvature is encoded in the parameter λ, which introduces corrections to the flat-space spectrum through terms proportional to λ, λ^2, and combinations involving the magnetic length l_B and topological index τ.

At $\lambda=0$, the energy spectrum reduces to the well-known relativistic Landau levels of graphene in flat space, reaffirming consistency with existing literature. However, for nonzero curvature ($\lambda>0$), the spectrum is no longer linear in quantum numbers, and curvature-dependent terms cause level shifts that grow with both n (Landau level index) and l (angular momentum). The square root structure ensures that the energy remains bounded from below, but the spacing between levels becomes nonuniform, indicating the emergence of curvature-induced confinement or stretching of the spectrum.

The τ parameter further breaks symmetry between particle and antiparticle branches, manifesting physically as an asymmetry in energy levels that could correspond to valley polarization or parity breaking in curved space. Notably, the appearance of mixed terms like $(4n(n+1))$ and $(2-\tau)l$ implies that quantum corrections grow more rapidly with excitation number than in the flat case, suggesting that higher energy states are more sensitive to the underlying geometry.

Overall, the obtained energy spectrum shows that AdS curvature not only lifts degeneracies and alters level spacing, but also encodes deeper topological and geometric features of the graphene system. This highlights the rich interplay between relativistic dynamics, curvature effects, and quantum structure in graphene subjected to strong fields in a curved background.

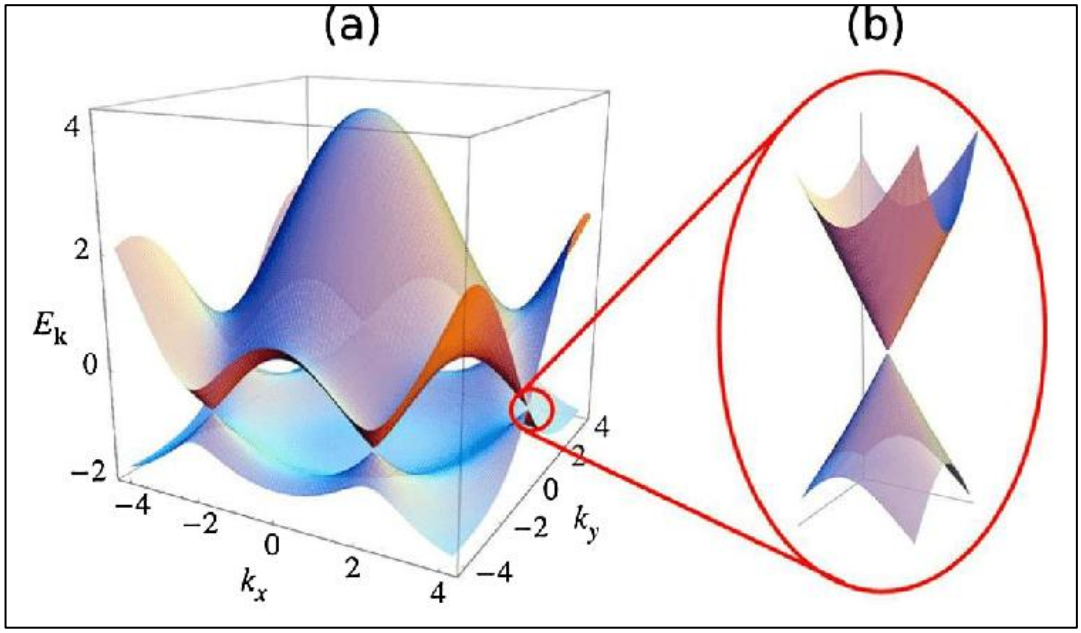

Figure 4-1: Graphene energy band structure (a) and the linear energy dispersion around the Fermi Energy (b).

4.3 Wave function discussion

The derived wave function $\Psi_n(r,\varphi)$ describes the quantum states of charge carriers in graphene under the influence of both a magnetic field and a curved (AdS) background geometry. Its form reflects the interplay between geometry, topology, and the relativistic dynamics of Dirac fermions in two dimensions.

The angular dependence through the term $e^{-il\varphi}$ confirms the conservation of angular momentum and the cylindrical symmetry of the system. The radial part incorporates a deformed measure $(1-\lambda r^2)^{\mu/2}$, a hallmark of AdS curvature, which alters the probability density distribution compared to the flat-space case. This deformation acts as a natural cutoff, ensuring that the wave function vanishes at the AdS boundary and remains normalizable.

The factor $(\lambda r^2)^{\nu/2}$introduces additional curvature-dependent scaling that modulates the localization of the wave function — smaller values of λ lead to flatter, more extended states, while larger curvature compresses the wave function toward the origin. The presence of the Jacobi polynomial $P_n^{(\mu, \nu-1/2)}$ captures the quantization of the system and encodes the radial excitations. These polynomials, modified by curvature-dependent parameters, ensure orthogonality and completeness under the curved metric.

Overall, this wave function reflects how AdS curvature not only modifies the spectrum but also reshapes the spatial structure of quantum states. The result reveals how the geometric background can confine, localize, or even destabilize electronic wave functions in curved-space graphene, providing a deep connection between geometry and quantum field behavior in condensed matter systems.

4.4 Thermodynamic Properties

The partition function, encodes the statistical behavior of graphene's charge carriers in a curved Anti-de Sitter (AdS) space under the influence of a magnetic field. This expression reflects how geometry (via the AdS curvature λ) and thermal effects (via temperature T) combine to shape the thermodynamic properties of the system.

The prefactor, involving $(\hbar V_F/l_B k_B T)^2$, arises from the density of states and energy level structure of Dirac quasiparticles in a magnetic field. The denominator includes a curvature correction via the $(1+\lambda l_B^2 \tau)^2$ term, demonstrating how the AdS geometry affects the effective energy spacing and density of states.

The correction inside the square brackets introduces a temperature-dependent term proportional to λT, showing how curvature modifies thermal fluctuations. As $\lambda \to 0$, the expression reduces to the known flat-space partition function, ensuring consistency with standard results.

Physically, this partition function determines how accessible quantum states contribute to the system's thermodynamics. It allows one to derive key quantities such as the free energy, entropy, internal energy, and heat capacity. The curvature-dependent corrections reveal how AdS geometry influences the thermal response of graphene, especially at high temperatures or in regimes of strong curvature.

Let’s analyze the plots of the thermodynamic properties starting with the partition function;

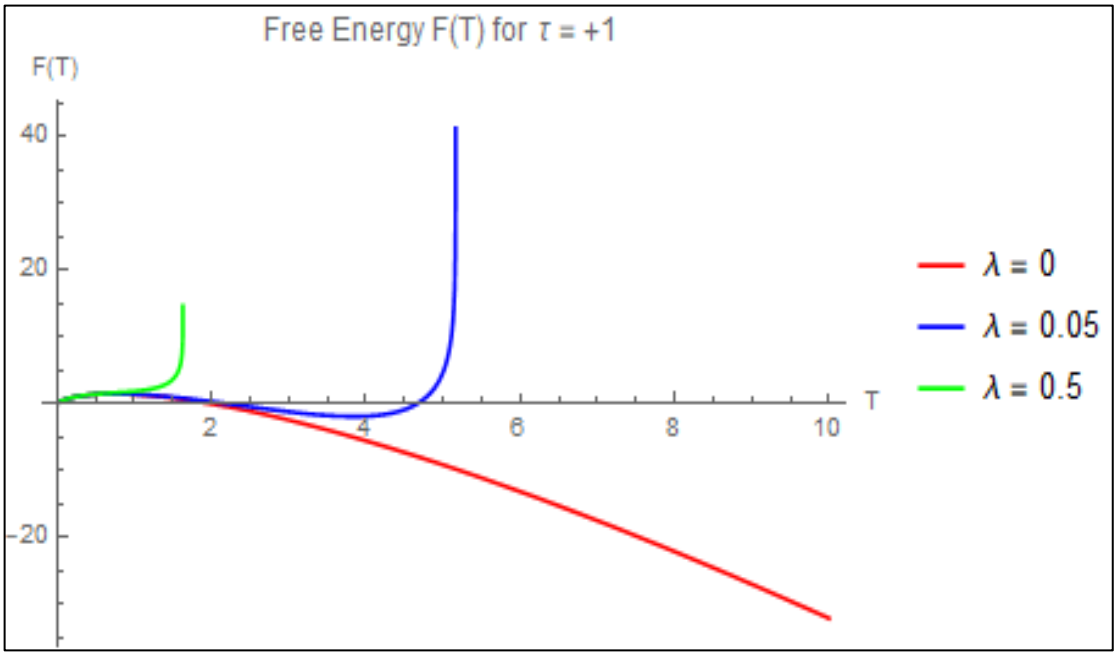

Figure 4-2: Free energy behavior with temperature for various deformation parameters under τ=+1.

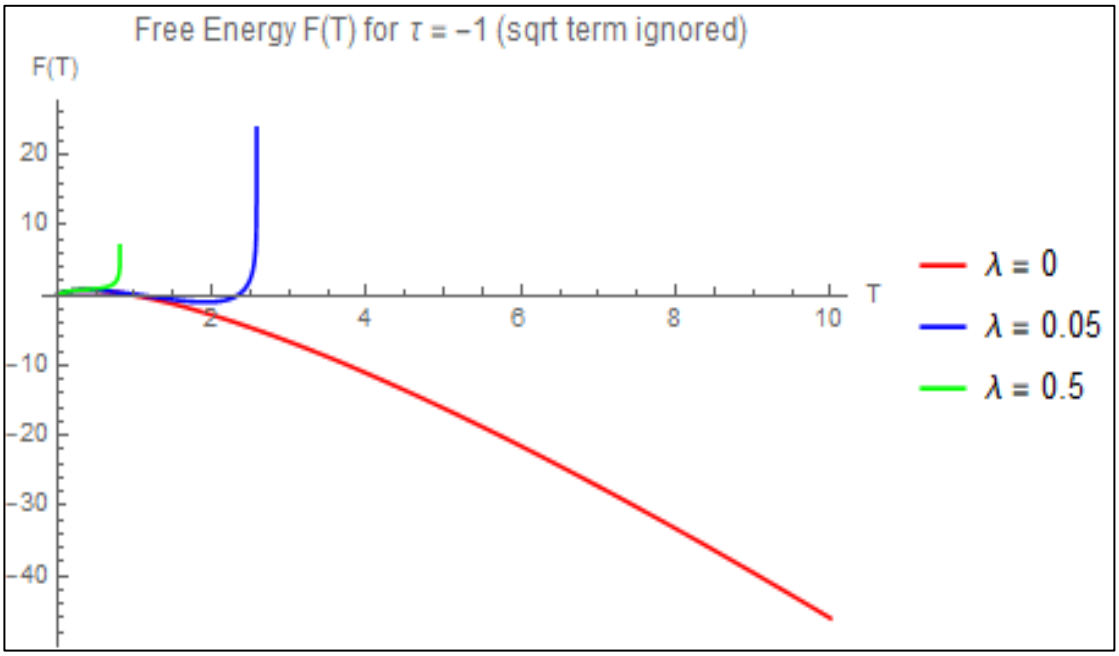

Figure 4-3: Free energy F(T) behavior with temperature for various deformation parameters under τ=-1.

The thermal behavior of the Graphene field in Anti-de Sitter (AdS) space is illustrated through the free energy $F(T)=-k_B T\ln(Z)$, plotted as a function of temperature for different values of the coupling parameter λ and curvature parameter τ. For $\tau=+1$, corresponding to positive curvature, the free energy exhibits a smooth, monotonically decreasing profile in the absence of coupling ($\lambda=0$), consistent with standard thermodynamic expectations. However, introducing a finite coupling ($\lambda=0.05$ and $\lambda=0.5$) induces divergences at specific critical temperatures. These divergences signify the vanishing of the partition function, marking the onset of thermodynamic instability. The critical temperature decreases as the coupling strength increases, reflecting the growing influence of interaction effects on the thermal stability of the system. A similar trend is observed for $\tau=-1$, representing negative curvature, where the free energy also diverges for non-zero coupling, but at lower temperatures compared to the $\tau=+1$ case. This indicates that negative curvature enhances the system's sensitivity to thermal and interaction effects. Notably, due to singular behavior in the partition function for $\tau=-1$, the geometric square root term was regularized in the computation. Overall, these results demonstrate that both the curvature of spacetime and the coupling strength play crucial roles in governing the thermal stability of Graphene fields in AdS backgrounds.

Let's move to the internal energy of the graphene in AdS, it's plot as below

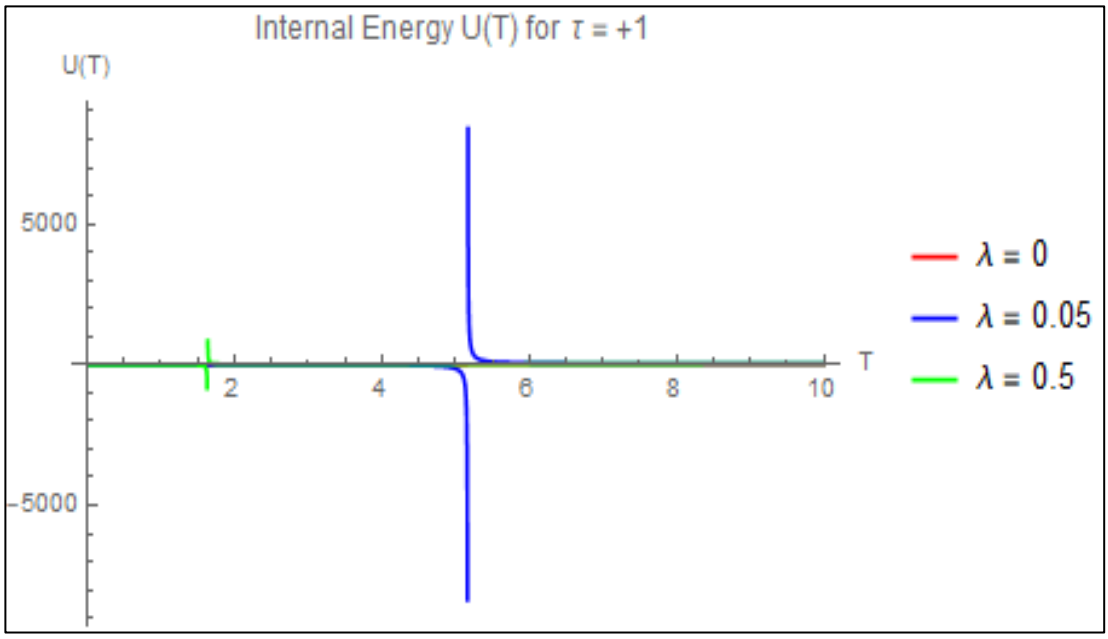

Figure 4-4: Mean Energy U(T) as a function of temperature for various deformation parameters under $\tau=+1$.

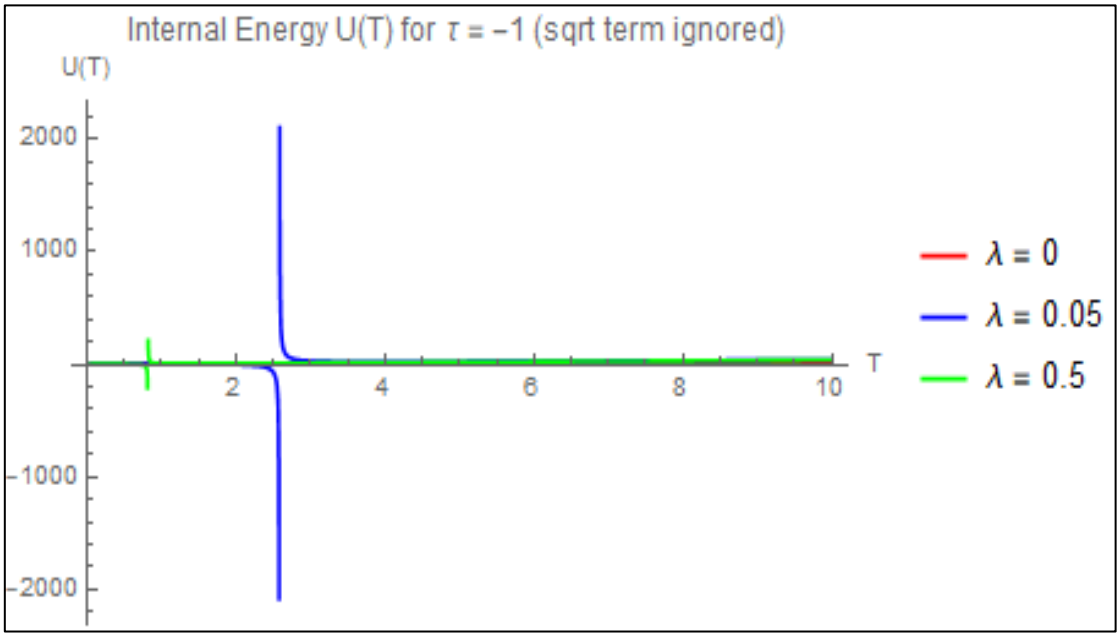

Figure 4-5: Mean energy U(T) as a function of temperature for various deformation parameters under τ=-1.

The internal energy $U(T)=k_BT^2 d\ln(Z)/ dT$ provides insight into the thermal excitation and response of the Dirac field in AdS space. For τ=+1, representing positive curvature, the internal energy remains regular and smoothly increasing in the case of no coupling (λ=0), reflecting typical thermodynamic behaviour. However, for finite couplings (λ=0.05 and λ=0.5), the internal energy exhibits distinct divergences at critical temperatures, corresponding to the points where the partition function approaches zero. These divergences indicate thermodynamic instability and signal the breakdown of the system's thermal equilibrium beyond specific coupling-dependent thresholds. Notably, the divergence for λ=0.05 occurs at a higher temperature than that for λ=0.5, highlighting the increasing destabilization with stronger coupling.

In the case of τ=−1, which corresponds to negative curvature, the internal energy was computed by simplifying the partition function to avoid the divergence associated with the vanishing square root term. Despite this simplification, the qualitative behaviour remains consistent: the red curve (λ=0) grows smoothly, while the blue and green curves (λ=0.05, λ=0.5) show sharp poles at lower critical temperatures than their τ=+1 counterparts. This implies that negative curvature enhances the thermal sensitivity of the system, reducing the threshold temperature for instability. In both cases, the divergences in internal energy coincide with the loss of physical meaning in the free energy and partition function, reinforcing the interpretation of these points as critical thermal limits. The dependence of these divergences on both the curvature and coupling strength

underscores the interplay between geometry and interaction effects in the thermodynamics of quantum fields in curved spacetimes.

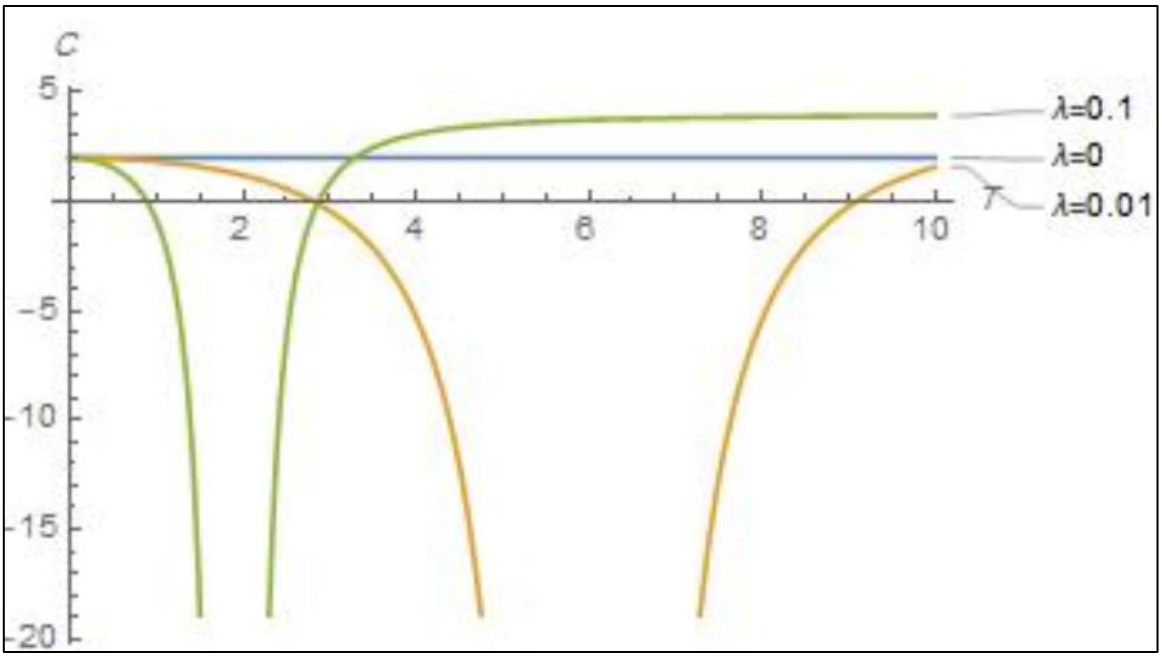

Figure 4-6: Specific heat C(T) as a function of temperature for various deformation parameters under τ=+1.

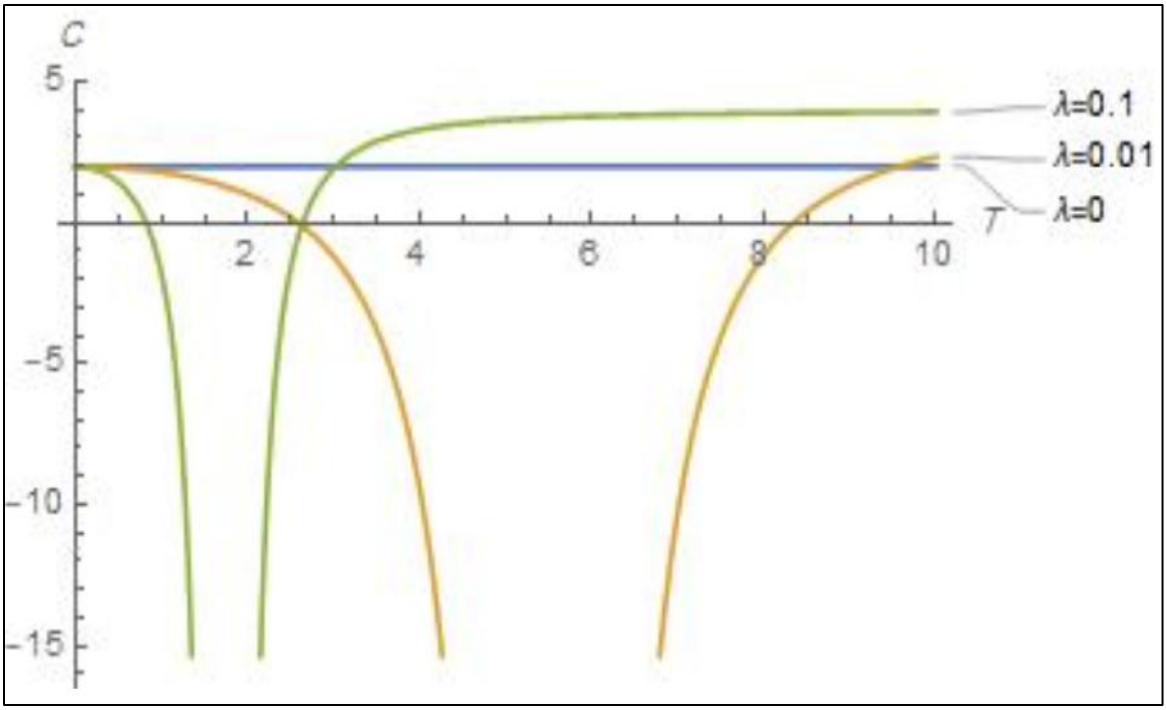

Figure 4-7: Specific heat C(T) as a function of temperature for various deformation parameters under τ=-1.

The heat capacity C(T), a measure of the system's response to thermal excitations, serves as a sensitive indicator of underlying thermodynamic stability and critical phenomena in graphene-like Dirac materials embedded in curved spacetime. In this study, the analysis is carried out for a Dirac field in an Anti-de Sitter (AdS) background, which introduces a curvature-dependent term controlled by the parameter τ. Two distinct curvature configurations $\tau=+1$ and $\tau=-1$ are considered, each with varying values of the coupling parameter λ, which encapsulates the interaction strength between the Dirac fermions and an external field (or geometric deformation). In the absence of interactions ($\lambda=0$), the heat capacity remains positive and flat across the entire temperature domain, consistent with the expected behaviour of non-interacting relativistic fermions. This baseline reflects a stable thermodynamic regime with no phase transitions or instabilities. However, the introduction of a non-zero coupling ($\lambda=0.01$ and $\lambda=0.1$) induces stark deviations. The most prominent feature is the appearance of divergent spikes (vertical asymptotes) at specific critical temperatures, beyond which the heat capacity turns negative and eventually diverges again. These divergences are thermodynamic signatures of instabilities or critical transitions driven by the interaction strength.

For $\tau=+1$, corresponding to a positively curved AdS background, the divergences in C(T) occur at lower temperatures for higher λ. This suggests that the interaction renders the system unstable at increasingly lower thermal energies. In physical terms, this implies that stronger interactions suppress the thermal robustness of the graphene-like Dirac system, potentially leading to a breakdown of equilibrium or a phase transition to a non-perturbative state.

Conversely, in the case of $\tau=-1$, which corresponds to a negatively curved AdS space, the same qualitative behaviour is observed, but with critical temperatures shifted to higher values. This indicates that negative curvature helps stabilize the system against thermally induced transitions, allowing it to maintain thermodynamic integrity over a broader temperature range. The comparative shift in divergence points between the $\tau=+1$ and $\tau=-1$ plots reinforces the interpretation that spacetime geometry directly modulates the thermal behaviour of Dirac quasiparticles in graphene-like systems.

Furthermore, the transition to negative heat capacity following the divergence reflects a regime where the system loses energy upon heating—a hallmark of metastability or collapse in gravitational or strongly correlated quantum systems. In condensed matter terms, this could signal a transition from a delocalized (Dirac) state to a localized or symmetry-broken phase, modulated by both thermal energy and curvature.

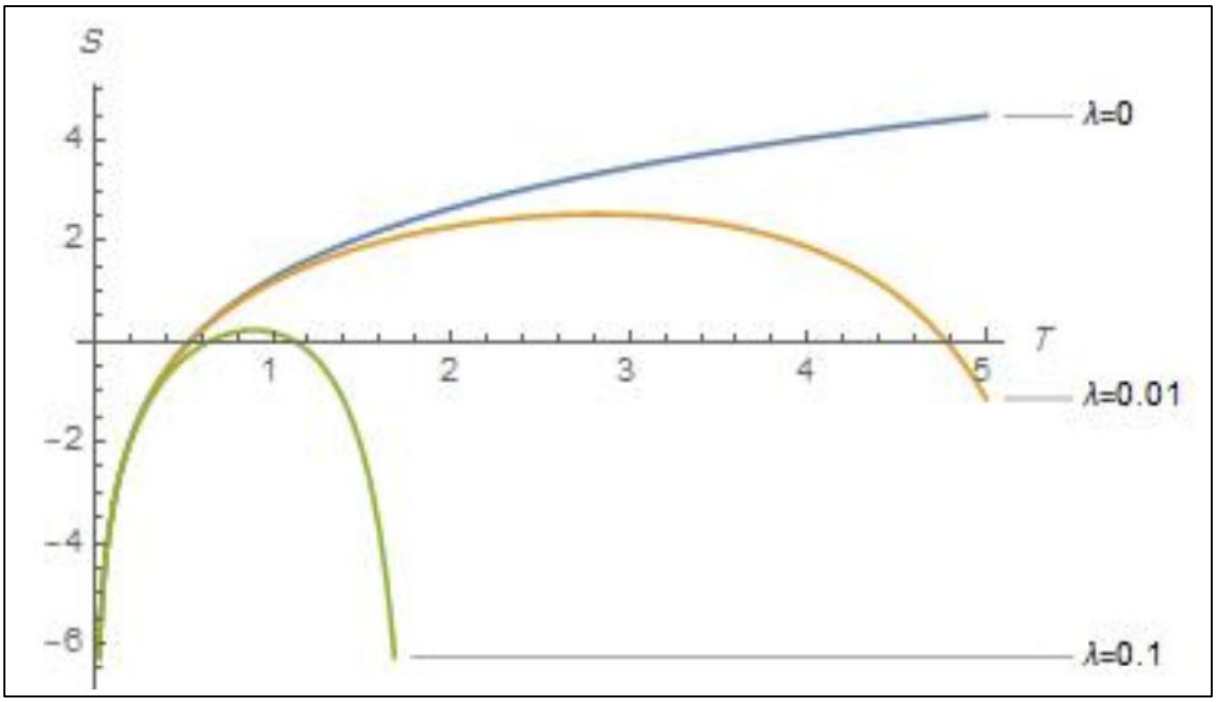

Figure 4-8: Entropy S(T) as a function of temperature for various deformation parameters under τ=+1.

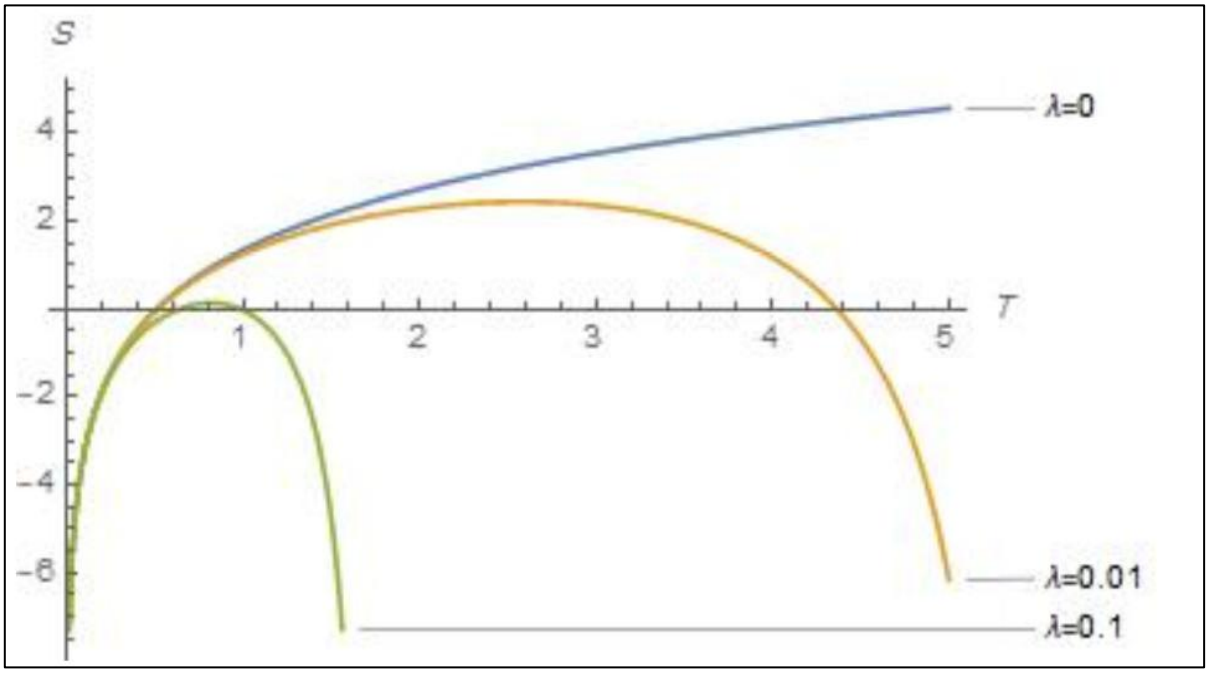

Figure 4-9: Entropy S(T) as a function of temperature for various deformation parameters under τ=-1.

The entropy S(T) provides a direct measure of the number of accessible microstates as a function of temperature, and is thus a crucial thermodynamic quantity for understanding the statistical

behaviour of graphene-like Dirac fields in curved backgrounds. In the present case, the system is studied within an Anti-de Sitter (AdS) geometry, incorporating curvature effects through the parameter τ\tauτ and interaction effects through the coupling constant λ\lambdaλ. The plots illustrate how entropy varies with temperature for both τ=+1 and τ=−1, and for three representative values of λ= 0, 0.01, and 0.1.

For λ=0, the system behaves as an ideal (non-interacting) Dirac gas, with the entropy increasing monotonically with temperature. This smooth, positive trend reflects the steady increase in the number of thermally accessible states, as expected in a well-behaved quantum field theory in curved space. Notably, this baseline behaviour is consistent across both curvature cases (τ=+1 and τ=−1), affirming that in the absence of interactions, curvature alone does not introduce thermodynamic instability.

As the coupling λ is turned on, a fundamentally different behaviour emerges. For both signs of curvature, the entropy curve initially follows the non-interacting case at low temperatures but then peaks and drops sharply as temperature increases. Eventually, S(T) becomes negative, and finally diverges to $-\infty$ at a finite critical temperature. This pathological behaviour originates from the structure of the partition function, which becomes ill-defined as its argument approaches zero—effectively signalling a breakdown of statistical equilibrium. Physically, this corresponds to a loss of well-defined thermodynamic microstates, a situation analogous to instability or a critical phase transition.

Interestingly, the location of the entropy divergence depends on both the coupling strength and the curvature. For higher λ, the divergence occurs at lower temperatures, indicating that strong interactions induce instability at earlier stages of thermal excitation. Comparing the two plots, we observe that the divergence for τ=−1 (negative curvature) is slightly delayed relative to the τ=+1 case, implying that negative curvature contributes a stabilizing effect. This mirrors the behaviour observed in the heat capacity and reinforces the idea that spacetime curvature and interaction strength jointly determine the thermodynamic bounds of graphene-like systems in AdS backgrounds.

General Conclusion

In this study, we have theoretically investigated the thermodynamic and quantum spectral properties of graphene-like Dirac fermions embedded in Anti-de Sitter (AdS) space, incorporating both geometric curvature and a coupling interaction parameter. By modeling the system with effective field theory and solving the resulting equations through analytical techniques—including the Nikiforov–Uvarov (NU) method—we have gained comprehensive insight into how deformations of spacetime geometry affect both the energy spectrum and thermal response of Dirac systems such as graphene.

From a thermodynamic perspective, the presence of AdS curvature leads to significant deviations from flat-space behavior. Key thermal quantities—free energy, internal energy, entropy, and heat capacity—were derived and analyzed for varying curvature (via the parameter $\tau=\pm1$) and interaction strength λ. We observed that while the system remains thermodynamically stable in the absence of coupling, the introduction of interaction generates critical phenomena such as divergences and negative entropy regions. These features are clear indicators of thermal instability, potentially signaling curvature-induced transitions or a breakdown of equilibrium. Positive curvature ($\tau=+1$) generally lowers the critical temperature and compresses thermodynamic stability, whereas negative curvature ($\tau=-1$) delays the onset of divergence, thus exhibiting a stabilizing influence.

The study further extended into the quantum domain by deriving the energy spectrum of the Graphene system in AdS space using the NU method. The resulting expression, Equation (2.85), reveals that both curvature and coupling substantially reshape the spectrum. Specifically, AdS curvature modifies the effective cyclotron-like quantization by introducing a geometry-dependent factor under the square root, and the coupling λ lifts the degeneracy of Landau levels and introduces nonlinear contributions. These effects break the equidistant nature of the spectrum, creating curvature- and coupling-induced level splitting. Notably, the curvature controls the spacing and stability of the energy levels: positive curvature compresses and destabilizes them, while negative curvature provides effective confinement and spreads the levels, reinforcing thermal and quantum stability.

The wavefunctions associated with these states, derived from orthogonal polynomials inherent in the NU method, also encode the effects of AdS geometry. The curvature modulates the shape and localization of these wavefunctions, with positive curvature leading to tighter spatial confinement and negative curvature allowing greater delocalization. These modifications influence observable quantities such as transition amplitudes, tunneling probabilities, and density of states.

In conclusion, this work demonstrates that both the geometric properties of spacetime and the interaction dynamics play a profound role in shaping the thermodynamic and quantum behavior of graphene-like systems. It bridges concepts from curved space quantum field theory**,** condensed matter physics, and AdS/CMT duality, offering a unified theoretical framework for understanding Dirac materials in deformed geometries. The results presented here not only contribute to the theoretical foundations of graphene in curved backgrounds but also open promising avenues for experimental analogs in strained graphene, curved substrates, and synthetic gauge fields in optical lattices.

References

[1] A. H. Castro Neto et al., "The electronic properties of graphene," *Rev. Mod. Phys.* **81**, 109 (2009).

[2] M. I. Katsnelson, *Graphene: Carbon in Two Dimensions*, Cambridge University Press (2012).

[3] F. Guinea, M. I. Katsnelson, and A. K. Geim, "Energy gaps and a zero-field quantum Hall effect in graphene by strain engineering," *Nature Physics* **6**, 30–33 (2010).

[4] A. Fasolino, J. H. Los, and M. I. Katsnelson, "Intrinsic ripples in graphene," *Nature Materials* **6**, 858–861 (2007).

[5] A. Cortijo and M. A. H. Vozmediano, "Effects of topological defects and local curvature on the electronic properties of planar graphene," *Nucl. Phys. B* **763**, 293–308 (2007).

[6] N. D. Birrell and P. C. W. Davies, *Quantum Fields in Curved Space*, Cambridge University Press (1982).

[7] S. A. Hartnoll, "Lectures on holographic methods for condensed matter physics," *Class. Quant. Grav.* **26**, 224002 (2009).

[8] S. Sachdev, "What can gauge-gravity duality teach us about condensed matter physics?" *Annu. Rev. Condens. Matter Phys.* **3**, 9–33 (2012).

[9] I. I. Cotaescu and E. Sporea, "Dirac fermions in de Sitter and Anti-de Sitter backgrounds: A comparative study," *Eur. Phys. J. C* **76**, 102 (2016).

[10] C. Furtado, F. Moraes, and A. M. de M. Carvalho, "Landau levels in graphene with topological defects," *Phys. Lett. A* **372**, 5368–5371 (2008).

[11] Geim, A. K., & Novoselov, K. S. (2007). The rise of graphene. Nature Materials, 6(3), 183–191.

[12] Novoselov, K. S., et al. (2004). Electric field effect in atomically thin carbon films. Science, 306(5696), 666–669.

[13] Castro Neto, A. H., et al. (2009). The electronic properties of graphene. Reviews of Modern Physics, 81(1), 109.

[14] Schwierz, F. (2010). Graphene transistors. Nature Nanotechnology, 5(7), 487–496.

[15] Bonaccorso, F., et al. (2010). Production and processing of graphene and 2D crystals. Materials Today, 15(12), 564–589.

[16] Dresselhaus, M. S., et al. (2010). Physics of Graphene. Springer.
[17] Wallace, P. R. (1947). The band theory of graphite. Physical Review, 71(9), 622.
[18] Oostinga, J. B., et al. (2008). Gate-induced insulating state in bilayer graphene devices. Nature Materials, 7(2), 151–157.
[19] Zhang, F., et al. (2011). Band structure of trilayer graphene. Physical Review B, 84(3), 035409.
[20] Balandin, A. A., et al. (2008). Superior thermal conductivity of single-layer graphene. Nano Letters, 8(3), 902–907.
[21] Seol, J. H., et al. (2010). Two-dimensional phonon transport in supported graphene. Science, 328(5975), 213–216.
[22] Ghosh, S., et al. (2010). Dimensional crossover of thermal transport in few-layer graphene. Nature Materials, 9(7), 555–558.
[23] Nair, R. R., et al. (2008). Fine structure constant defines visual transparency of graphene. Science, 320(5881), 1308.
[24] Koppens, F. H. L., et al. (2014). Photodetectors based on graphene, other two-dimensional materials and hybrid systems. Nature Nanotechnology, 9(10), 780–793.
[25] Ni, Z. H., et al. (2007). Optical reflection and transmission properties of graphene. Nano Letters, 7(9), 2758–2763.
[26] Bouhafs, D., et al. (2021). Influence of layer number and growth temperature on optical properties of graphene. Journal of Applied Physics, 129(3), 033101.
[27] Lee, C., et al. (2008). Measurement of the elastic properties and intrinsic strength of monolayer graphene. Science, 321(5887), 385–388.
[28] Pei, S., & Cheng, H.-M. (2012). The reduction of graphene oxide. Carbon, 50(9), 3210–3228.
[29] Parvez, K., et al. (2014). Electrochemically exfoliated graphene as solution-processable, highly conductive electrodes. ACS Nano, 8(1), 235–246.
[30] Li, X., et al. (2009). Large-area synthesis of high-quality and uniform graphene films on copper foils. Science, 324(5932), 1312–1314.
[31] Maldacena, J. M. (1998). The large N limit of superconformal field theories and supergravity. Advances in Theoretical and Mathematical Physics, 2(2), 231–252.
[32] Kempf, A., Mangano, G., & Mann, R. B. (1995). Hilbert space representation of the minimal length uncertainty relation. Physical Review D, 52(2), 1108.

[33] Das, S., & Vagenas, E. C. (2008). Universality of Quantum Gravity Corrections. Physical Review Letters, 101(22), 221301.

[34] Hossenfelder, S. (2013). Minimal length scale scenarios for quantum gravity. Living Reviews in Relativity, 16(1), 2.

[35] Vafek, O. (2007). Thermodynamics of the low-energy excitations of graphene. *Physical Review Letters*, 98(21), 216401.

[36] Nika, D. L., & Balandin, A. A. (2012). Two-dimensional phonon transport in graphene. *Journal of Physics: Condensed Matter*, 24(23), 233203.

[37] Müller, M., Fritz, L., & Sachdev, S. (2009). Quantum-critical relativistic magneto transport in graphene. *Physical Review B*, 78(11), 115406.

[38] Fong, K. C., & Schwab, K. C. (2012). Ultrasensitive and wide-bandwidth thermal measurements of graphene at low temperatures. *Physical Review X*, 2(3), 031006.

[39] Huang, X., et al. (2009). Thermodynamic properties of Dirac fermions in graphene. *Physica B: Condensed Matter*, 404(15-16), 2259–2263.

[40] Zuev, Y. M., Chang, W., & Kim, P. (2009). Thermoelectric and magneto thermoelectric transport measurements of graphene. *Physical Review Letters*, 102(9), 096807.

[41] Mignemi, S. (2012). Classical and quantum mechanics of the nonrelativistic Snyder model in curved space. Classical and Quantum Gravity, 29(21), 215019.

[42] Stetsko, M. M. (2015). Dirac oscillator and nonrelativistic Snyder-de Sitter algebra. Journal of Mathematical Physics, 56(1), 012101.

[43] Bolen, B., & Cavaglia, M. (2005). (Anti-) de Sitter black hole thermodynamics and the generalized uncertainty principle. General Relativity and Gravitation, 37(7), 1255-1262.

[44] Egrifes, H., Demirhan, D., & Büyükkiliç, F. (1999). Exact solutions of the Schrödinger ¼ equation for two "deformed" hyperbolic molecular potentials. Physica Scripta, 60(3), 195.

[45] Nikiforov, A. F., & Uvarov, V. B. (1988). Special functions of mathematical physics (Vol. 205). Basel: Birkhuser.

[46] Pacheco, M. H., Landim, R. R., & Almeida, C. A. S. (2003). One-dimensional Dirac oscillator in a thermal bath. Physics Letters A, 311(2-3), 93-96.